

Spin-flip processes and radiative decay of dark intravalley excitons in transition metal dichalcogenide monolayers

A. O. Slobodeniuk¹ and D. M. Basko²

¹*Laboratoire National des Champs Magnétiques Intenses, CNRS-UGA-UPS-INSA-EMFL, 25 avenue des Martyrs, 38042 Grenoble, France*

²*Laboratoire de Physique et Modélisation des Milieux Condensés, Université de Grenoble-Alpes and CNRS, 25 rue des Martyrs, 38042 Grenoble, France*

We perform a theoretical study of radiative decay of dark intravalley excitons in transition metal dichalcogenide monolayers. This decay necessarily involves an electronic spin flip. The intrinsic decay mechanism due to interband spin-flip dipole moment perpendicular to the monolayer plane, gives a rate about 100–1000 times smaller than that of bright excitons. However, we find that this mechanism also introduces an energy splitting due to a local field effect, and the whole oscillator strength is contained in the higher-energy component, while the lowest-energy state remains dark and needs an extrinsic spin-flip mechanism for the decay. Rashba effect due to a perpendicular electric field or a dielectric substrate, gives a negligible radiative decay rate (about 10^7 times slower than that of bright excitons). Spin flip due to Zeeman effect in a sufficiently strong in-plane magnetic field can give a decay rate comparable to that due to the intrinsic interband spin-flip dipole.

I. INTRODUCTION

Transition metal dichalcogenides (TMDCs) are layered materials with the chemical composition MX_2 , where M is a transition metal element (such as molybdenum or tungsten), and X is a chalcogen (sulfur, selenium, or tellurium). The interest to semiconducting TMDCs has been sparked by the recent discovery of the monolayer MoS_2 being a direct-gap semiconductor, in contrast to its bulk indirect-gap counterpart [1, 2]. Atomically thin TMDC monolayers can be extracted from bulk crystals by exfoliation, similarly to graphene [1–3], or grown by molecular beam epitaxy or chemical vapor deposition [4–6]. The optical gap in the visible light range [1, 2] and tightly bound excitons [7–13], make them quite promising for optical applications [14].

A unique feature of TMDCs is the so-called spin-valley locking [15]. The conduction and valence band extrema are located at the two inequivalent $\pm\mathbf{K}$ points (valleys) of the hexagonal first Brillouin zone. Absence of inversion symmetry and strong spin-orbit interaction, originating from d -orbitals of the metal atoms, leads to spin splitting of the bands. The sign of the splitting is opposite in the two valleys, as required by the time-reversal symmetry, so the lowest-energy electron and hole states have opposite spin projections in the opposite valleys, as shown schematically in Fig. 1. It is important that the two valleys can be addressed separately by optical means. Namely, in each valley optical transitions with only one of the two in-plane circular polarizations are allowed [15–17]. This opens an exciting perspective of manipulating the spin/valley degree of freedom optically [18–24].

The large spin splitting in the valence band (a fraction of eV) gives rise to two prominent features in the absorption spectrum, called A and B excitons, formed by a hole in the upper or lower spin-split valence band, respectively, and an electron in the conduction band. The spin splitting in the conduction band is much weaker (on the

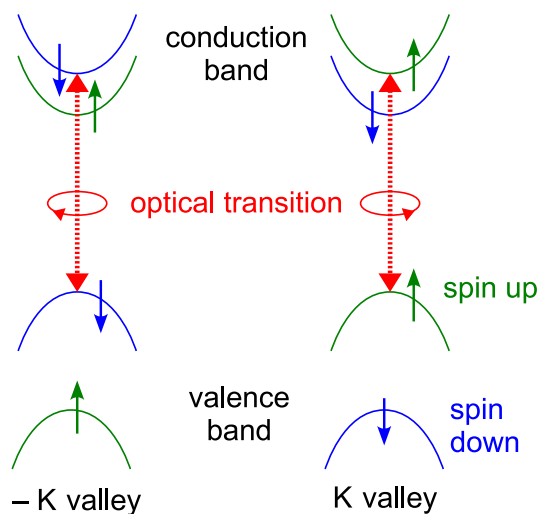


FIG. 1. A schematic view of the conduction and valence band extrema of a tungsten-base TMDC monolayer. The solid arrows show the spin projections. In molybdenum-based compounds, the spin projections in the conduction band are the opposite. The dashed arrows represent circularly polarized optical transitions for A excitons in each valley.

meV scale); moreover, its sign depends on the material: in molybdenum-based compounds, the top valence band and the lowest conduction band have the same spin projection in the same valley, while in tungsten-based ones, they are opposite (Fig. 1) [25–27]. This implies that the lowest-energy A excitons in WX_2 involve electronic states either from the same valley but with opposite spins, or with the same spin but from different valleys. As the photons, polarized in the plane, couple only to the orbital degrees of freedom and carry a very small momentum, they are decoupled from such excitons, which therefore have been named “dark”. This picture provided a nat-

ural explanation of the experimentally observed rise of the luminescence intensity in WSe_2 with increasing temperature in terms of the increasing thermal population of the higher-energy bright A excitons [28–31]. At sufficiently low temperatures, several peaks at energies below the neutral and charged bright A excitons have been seen in the WSe_2 luminescence spectrum [21, 22, 28, 32–36].

These observations pose an important question about existence of possible mechanisms for radiative decay of the dark excitons. While the radiative decay of bright excitons in TMDCs fits in the standard picture for 2D excitons [37–39] and has been described in several theoretical works [40–43], the dark exciton radiative decay requires unlocking the spin and the valley degrees of freedom. Namely, for intervalley dark excitons, a large momentum should be provided to the electron or to the hole without flipping its spin, which requires a third body (a phonon, an impurity, another electron or a hole). For intravalley dark exciton decay, a spin flip is required. Investigation of this latter possibility is the subject of the present work.

In this paper, we give an estimate of the intravalley dark exciton radiative decay rate due to several spin-flip mechanisms (see Sec. IV C for the final expressions and estimates). One such mechanism could be the Bychkov-Rashba effect [44], as mentioned in [45]. It requires breaking of the crystal symmetry with respect to reflection in the monolayer plane. This can be achieved by applying an external electric field, perpendicular to the plane; the corresponding Rashba coefficient has been calculated in [46]. The reflection symmetry can also be broken if the dielectric environments on the two sides of the monolayer are different. Having not found any information on the magnitude of this effect in the literature, we make our own crude estimate; for a TMDC monolayer on a glass-like substrate with vacuum above, we obtain an equivalent electric field to be roughly of the order of $0.1 \text{ V}/\text{\AA}$. However, even for this relatively high field, the resulting radiative rate is about 10^{-7} of the bright exciton decay rate Γ_0 , which makes the Rashba mechanism totally negligible with respect to other relaxation processes. The main reason for this is that Rashba spin-flip amplitude is proportional to the electron momentum, and radiative decay is possible only in a narrow radiative region of small momenta. Another way to flip the electron spin is to apply an in-plane magnetic field and use the Zeeman effect. It is momentum-independent, and for a quite high but still realistic field of 30 T we obtain a radiative rate exceeding $10^{-3}\Gamma_0$.

Finally, we analyzed the intrinsic radiative decay mechanism due to the interband spin-flip dipole moment perpendicular to the monolayer plane, mentioned in [40, 47]. In fact, it is the presence of this dipole moment that gives rise to Bychkov-Rashba coupling in a perpendicular electric field [48], so its magnitude can be deduced from the estimates of [46] for the Rashba coefficient. This enabled us to estimate the associated radiative decay rate as $\sim (10^{-2} - 10^{-3})\Gamma_0$. However, we also found that the same

out-of-plane interband dipole gives rise to a Coulomb local-field term which lifts the double degeneracy between the dark excitons made of electronic states from the two valleys (the possibility of such splitting was briefly mentioned in [45]). This local-field effect is analogous to the exchange energy shift of the Z excitons in semiconductor quantum wells [38, 49], and produces an energy splitting which we very roughly estimate as about 10 meV . Its precise evaluation requires a microscopic treatment on the atomic scales, similar to that in [47]. Crucially, the whole oscillator strength of the interband spin-flip dipole goes into the higher-energy component. Thus, we find that the dark intravalley A exciton has, in fact, two components, one which is truly dark and the other one about $100\text{--}1000$ times darker than the bright exciton, so it can be called “dim”.

Although our results for the dark exciton splitting and decay rates apply both to molybdenum- and tungsten-based compounds (the discussed decay mechanisms work quite analogously in the two cases), in the context of photoluminescence (PL) our results are more relevant to the WX_2 case, where the dark excitons have lower energies and thus are more populated at low temperatures than the bright ones. Still, we are not yet in the position to unambiguously identify various peaks observed in the low-temperature PL spectra of WSe_2 [21, 22, 28, 32–36] as being due to dark or dim excitons. Our work focuses on intravalley spin-flip processes only, and a detailed theoretical study of various valley-flip processes is still required to create a complete picture. Still, our results give some indications for experimental studies which could shed some light on the origin of various features in the spectrum. For example, because of the dark-dim splitting, at low temperatures the emission from the dim exciton should be suppressed by an activation factor, analogously to that from the bright one, which should manifest itself in the temperature dependence of the relative peak intensities. The transition dipole of the dim component being perpendicular to the plane, it could be identified by the angular distribution of the emission. The dark component can be made decay by applying an in-plane magnetic field, and the corresponding rate can be made comparable to that of the dim component for a sufficiently high field.

The paper is organized as follows. In Sec. II we describe the effective model for electrons in the TMDC monolayer, the excitonic states, and specify how different spin-flip mechanisms enter the model. In Sec. III, we discuss spin-mixing of excitonic states and calculate the “mechanical” susceptibilities of the TMDC monolayer, which determine the exciton coupling to the macroscopic electromagnetic field. In Sec. IV we study the effect of the exciton coupling to the electromagnetic field and compute the radiative energy shifts and decay rates for the excitons. Finally, in Sec. V we summarize our results and discuss some of their implications and perspectives. Some details of calculations are presented in several appendices.

II. THE MODEL

We set $\hbar = 1$ throughout the paper, and write the electronic Hamiltonian of a TMDC monolayer as

$$\hat{H} = \hat{H}_b + \hat{H}_{ee} + \hat{H}_{sf}. \quad (1)$$

Its three terms will be discussed in the following subsections.

A. Electronic bands

We assume the monolayer to be in the xy plane, the three-dimensional position vector \mathbf{R} represented $\mathbf{R} \equiv (x, y, z) \equiv (\mathbf{r}, z)$, so that \mathbf{r} denotes the position in the monolayer plane. The first term in Eq. (1), \hat{H}_b , is the usual effective two-band Hamiltonian [50]

$$\hat{H}_b = \sum_{\tau=\pm 1} \int \hat{\psi}_{\tau}^{\dagger}(\mathbf{r}) \mathcal{H}_{\tau}(-i\nabla) \hat{\psi}_{\tau}(\mathbf{r}) d^2\mathbf{r}, \quad (2)$$

written in terms of four-component column operators $\hat{\psi}_{\tau} = [\hat{\psi}_{\tau,c,\uparrow} \hat{\psi}_{\tau,c,\downarrow} \hat{\psi}_{\tau,v,\uparrow} \hat{\psi}_{\tau,v,\downarrow}]^T$, where $\tau = \pm 1$ labels the two valleys $\pm\mathbf{K}$, and $\mathcal{H}_{\tau}(\mathbf{k})$ is the 4×4 matrix, written in the block form,

$$\mathcal{H}_{\tau}(\mathbf{k}) = \begin{bmatrix} E_g + \tau\Delta_c\sigma_z + \alpha_c k^2 & v(\tau k_x - ik_y) \\ v(\tau k_x + ik_y) & \tau\Delta_v\sigma_z - \alpha_v k^2 \end{bmatrix}. \quad (3)$$

Here σ_z is the third Pauli matrix in the spin subspace, E_g is the band gap, v is the velocity matrix element between the band extrema Bloch functions (which can be made real by an appropriate choice of the relative phase between the conduction and valence band Bloch functions). The coefficients $\alpha_{c,v}$ are related to the electron and hole effective masses $m_{e,h}$ as

$$\frac{1}{2m_{e,h}} = \alpha_{c,v} + \frac{v^2}{E_g}. \quad (4)$$

Typically, $E_g \sim 2.5 - 3$ eV, $v \sim 2.5$ eV $\cdot \text{\AA}$, $m_e \sim m_h \sim 0.5 m_0$ for MoX_2 and $\sim 0.3 m_0$ for WX_2 (m_0 being the free electron mass).

$\Delta_{c,v}$ in Eq. (3) is half of the spin splitting in the conduction/valence bands. We distinguish the $\pm\mathbf{K}$ valleys by assuming the valence band states to originate predominantly from the metallic orbitals with the z projections of the angular momentum equal to ± 2 at the $\pm\mathbf{K}$ point, respectively [15, 26, 51–58]. This fixes $\Delta_v > 0$, as well as the valley-dependent optical selection rules: the left/right circular polarisation can be absorbed in the $\pm\mathbf{K}$ valley, respectively, as the conduction band states originate mostly from zero-angular-momentum metallic orbitals and the angular momentum is conserved modulo 3 due to the three-fold crystal rotation symmetry. Typically, $\Delta_v \sim 100 - 200$ meV in MoX_2 and $400 - 500$ meV in WX_2 . Δ_c is much weaker, usually a few tens of meV,

with the exception of MoS_2 where it is extremely weak, ~ 3 meV. The sign of Δ_c depends on the material: $\Delta_c < 0$ ($\Delta_c > 0$) in molybdenum-based (tungsten-based) compounds. Because of this, the lowest-energy interband transition in tungsten-based compounds involves either a spin flip or valley switching.

B. Coulomb interaction and excitons

The second term in Eq. (1), \hat{H}_{ee} , represents the Coulomb interaction between electrons,

$$\hat{H}_{ee} = \frac{1}{2} \int V(\mathbf{r} - \mathbf{r}') \hat{\rho}(\mathbf{r}) \hat{\rho}(\mathbf{r}') d^2\mathbf{r} d^2\mathbf{r}', \quad (5)$$

$$\hat{\rho}(\mathbf{r}) = \sum_{\tau=\pm 1} \hat{\psi}_{\tau}^{\dagger}(\mathbf{r}) \begin{bmatrix} 1 & 1 \\ 1 & 1 \end{bmatrix} \hat{\psi}_{\tau}(\mathbf{r}). \quad (6)$$

Here each element of the block 2×2 matrix should be understood as the unit matrix in the spin space. The diagonal (intraband) blocks are responsible for direct electron-electron and hole-hole repulsion, while the off-diagonal blocks encode the direct electron-hole attraction, which gives rise to the excitonic bound state. We included only the intra-valley part of the electron density $\hat{\rho}(\mathbf{r})$, as it is the long-range part of the Coulomb interaction (on the scale of lattice constant) which is responsible for the exciton formation.

The wave function of the electron-hole relative motion, $\Phi(\mathbf{r}_e - \mathbf{r}_h)$, is obtained from the corresponding Schrödinger equation,

$$\left[-\frac{\nabla^2}{2m'} + V(\mathbf{r}) \right] \Phi(\mathbf{r}) = E \Phi(\mathbf{r}), \quad (7)$$

where $m' = m_e m_h / (m_e + m_h)$ is the reduced mass. The lowest eigenvalue $E = -E_b$ of Eq. (7) defines the exciton binding energy E_b . As we are working in the parabolic approximation for the electronic dispersion and assume the electron and the hole masses to be spin-independent, the wave function $\Phi(\mathbf{r})$ and the binding energy E_b are the same for all spin and valley configurations of the electron and the hole.

We do not specify the explicit form of the pair interaction potential $V(\mathbf{r})$, as we will not be solving Eq. (7). It is known that because of strong dielectric confinement in the TMDC monolayer, the interaction potential is not $1/r$, so the bound state wave functions do not have a hydrogenic form [8–12]. Instead, we will assume $\Phi(\mathbf{r})$ and E_b to be known and treat them as input parameters. In fact, we will not need the whole wave function $\Phi(\mathbf{r})$, but only its value $\Phi(0)$ at the coinciding electron and hole positions. By the order of magnitude, $\Phi(0)$ is the inverse radius of the excitonic bound state. Estimating it as $\Phi(0) \sim \sqrt{m'E_b}$ with the binding energy $E_b \sim 0.5 - 1$ eV [7–9], gives $\Phi(0) \sim 0.1 - 0.2 \text{\AA}^{-1}$, while from the measured diamagnetic shift of the exciton energy one infers values slightly below 0.1\AA^{-1} [59].

The contribution from the off-diagonal matrix elements in Eq. (6) corresponds to the exchange interaction between the electron and the hole. It will be taken into account in Sec. IV in the framework of macroscopic electrodynamics.

C. Spin-flip processes

The third term in Eq. (1), \hat{H}_{sf} , is the spin flip which arises when the reflection symmetry in the z direction is broken [44]. We write this term as [48]

$$\hat{H}_{sf} = -\mathcal{E}_z \sum_{\tau=\pm 1} \int \hat{\psi}_{\tau}^{\dagger}(\mathbf{r}) \mathcal{D}_{\tau} \hat{\psi}_{\tau}(\mathbf{r}) d^2\mathbf{r}, \quad (8)$$

$$\mathcal{D}_{\tau} = \begin{bmatrix} 0 & 0 & 0 & -id_z\delta_{\tau,-1} \\ 0 & 0 & -id_z\delta_{\tau,1} & 0 \\ 0 & id_z\delta_{\tau,1} & 0 & 0 \\ id_z\delta_{\tau,-1} & 0 & 0 & 0 \end{bmatrix}. \quad (9)$$

We assumed that the reflection symmetry is broken by an external perpendicular electric field \mathcal{E}_z , introduced explicitly. Then, by definition, the operator multiplying $-\mathcal{E}_z$ is nothing but the z component of the electric dipole moment operator. If there is no external electric field, but the reflection symmetry is broken by some other mechanism (e. g., van der Waals interaction with a dielectric substrate), the coupling Hamiltonian still has the form (8) which is fixed by the symmetry, but instead of $d_z\mathcal{E}_z$ its strength is determined by another parameter having the dimensionality of energy. For example, the parameter λ_{ext} from [48] is related to $d_z\mathcal{E}_z$ as $d_z\mathcal{E}_z = 2\lambda_{ext}$. The parameter d_z is real, which is fixed by the combination of time-reversal symmetry and the reflection symmetry $x \rightarrow -x$ (see Appendix A for details). The peculiar valley structure of the matrix \mathcal{D}_{τ} arises because the total angular momentum (orbital plus spin) is conserved modulo 3 due to the crystal symmetry: in \mathbf{K} ($-\mathbf{K}$) valley only spin-up (spin-down) states in the valence band can couple to only spin-down (spin-up) in the conduction band, the corresponding total angular momentum change being precisely ± 3 .

The intraband dipole spin-flip Hamiltonian (8) can be understood as a combination of the in-plane part $\hat{L}_+\hat{s}_- + \hat{L}_-\hat{s}_+$ of the atomic spin-orbit coupling $\propto \hat{\mathbf{L}} \cdot \hat{\mathbf{s}} = \hat{L}_z\hat{s}_z + (\hat{L}_+\hat{s}_- + \hat{L}_-\hat{s}_+)/2$ (here $\hat{\mathbf{L}}$ and $\hat{\mathbf{s}}$ are the orbital angular momentum and the spin of the electron, $\hat{L}_{\pm} \equiv \hat{L}_x \pm i\hat{L}_y$, $\hat{s}_{\pm} \equiv \hat{s}_x \pm i\hat{s}_y$) and of the electric potential $-e\mathcal{E}_z z$ which acts as a perturbation on the microscopic wave functions of the electron in the crystal [46]. For example, under the action of the $\hat{L}_+\hat{s}_-$ part of the atomic spin-orbit coupling, a spin-up electron in the conduction band can first perform a virtual transition to the next conduction band (denoted here by $c+1$), which flips its spin. It is crucial that the band $c+1$ is odd under the reflection $z \rightarrow -z$, since the conduction band is even, and the operators \hat{L}_{\pm} are odd, so the matrix elements $\langle c+1|\hat{L}_{\pm}|c\rangle$ are allowed. Next, the electron performs the

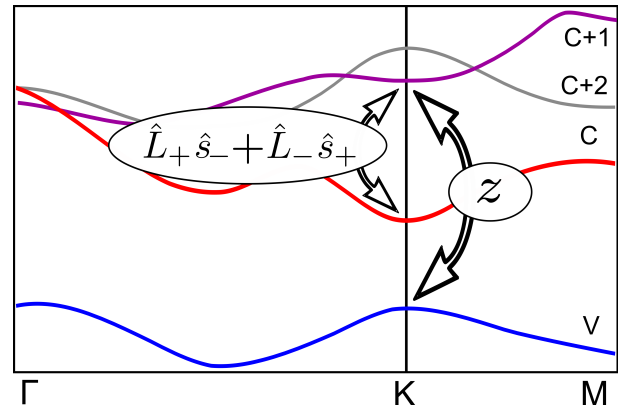


FIG. 2. A sketch of the TMDC monolayer band structure, including the valence band (v) and three lowest conduction bands (c, c+1, c+2). The arrows represent the virtual transitions which lead to the intraband dipole spin-flip transition, described by Eq. (8). The spin splitting of the bands is not shown for simplicity.

transition to the valence band, induced by the perturbation $-e\mathcal{E}_z z$. Again, because the valence band is even and z is odd, the matrix element $\langle v|z|c+1\rangle \neq 0$. The result of these two virtual processes is the transition from the conduction to the valence band, accompanied by the spin flip, as shown schematically in Fig. 2. Such transition is forbidden if there is no perturbation to break the parity $z \rightarrow -z$. Combining the interband Hamiltonian \hat{H}_{sf} with the off-diagonal terms in Eq. (3) in the first-order perturbation theory, one can project the spin-flip terms on the conduction and valence bands (see Appendix B). Upon projection, they acquire the familiar Rashba-type form [44], linear in momentum \mathbf{k} :

$$\mathcal{H}_{\tau}^R(\mathbf{k}) = \frac{v\mathcal{E}_z}{E_g} d_z [\mathbf{k} \times \boldsymbol{\sigma}]_z \begin{bmatrix} 1 & 0 \\ 0 & -1 \end{bmatrix}. \quad (10)$$

This form matches the one studied in [46] where the Rashba coupling strength was parametrized by λ_{BR} , related to $d_z\mathcal{E}_z$ as $id_z\mathcal{E}_z = \lambda_{BR}E_g/v$. The parameter $|\lambda_{BR}|$ was estimated in [46] for MoS₂, MoSe₂, WS₂, WSe₂ monolayers suspended in vacuum and subject to an external perpendicular electric field. This enables us to extract $|d_z/e|$ of about 0.02 Å, 0.03 Å, 0.06 Å, and 0.08 Å, for MoS₂, MoSe₂, WS₂, and WSe₂, respectively.

We are not aware of any estimates in the literature for the Rashba coupling strength induced by a dielectric substrate. Therefore, we make our own crude estimate of the effective electric field in Appendix C, which gives $\mathcal{E}_z \sim 0.1$ V/Å for a WX₂ monolayer lying on a glass-like substrate with a dielectric constant ~ 4 and vacuum above.

Finally, we note that in addition to Rashba effect in a perpendicular electric field, the spin can be flipped by the Zeeman effect if an in-plane magnetic field \mathbf{B}_{\parallel} is applied. This effect is taken into account straightforwardly by adding $g_{c,v}\mu_B\mathbf{B}_{\parallel} \cdot \boldsymbol{\sigma}/2$ to the diagonal matrix elements

in Eq. (3), where $\mu_B \approx 58 \mu\text{eV}/\text{T}$ is the Bohr magneton and $g_{c,v} \approx -2$ is the in-plane gyromagnetic ratio for electrons in the conduction and valence band.

D. Coupling to photons

The Hamiltonian of interaction between the electrons and the transverse photons, which are described by the long-wavelength vector potential $\mathbf{A}(\mathbf{r})$, is usually obtained from the requirement of gauge invariance by performing the Peierls substitution in Eq. (3): $\mathcal{H}_\tau(\mathbf{k}) \rightarrow \mathcal{H}_\tau(-i\nabla - (e/c)\mathbf{A})$. However, besides coupling to photons via gauge potentials, electrons can couple directly to electric and magnetic fields. Such terms are gauge invariant and cannot be deduced from the bare electronic Hamiltonian in the envelope function approximation, as they correspond to the effect of electromagnetic field on the microscopic Bloch functions.

In the previous subsection, we have already presented such terms, corresponding to Rashba and Zeeman effects. It is crucial for our analysis that, once the dipole operator in Eq. (8) is determined, it can also describe the electronic coupling to the photon field. Namely, \mathcal{E}_z can be understood not just as a static external field, but as the electric field of photons as well. In this case, one should write $\mathcal{E}_z = \mathcal{E}_z(\mathbf{r})$ and put it inside the space integral. The corresponding Hamiltonian can then describe interband photon absorption/emission, accompanied by the spin flip (the existence of such coupling was briefly mentioned in [40]).

III. POLARIZATION SUSCEPTIBILITY

A. General definitions

The main quantity which we use to describe the interaction of excitons with light is the susceptibility $\chi_{ij}(\mathbf{q}, \omega)$, defined as the mechanical response of the excitonic polarization to the electric field at the frequency ω and the in-plane wave vector \mathbf{q} . (The term ‘‘mechanical’’ implies that only the direct Coulomb interaction is taken into account for the moment; the exchange interaction will be included in the framework of macroscopic electrodynamics.) We define the polarization \mathbf{P} as the dipole moment per unit area. It is a three-dimensional vector, whose z component is defined via (8) as the operator multiplying $-\mathcal{E}_z$, while the in-plane components are most conveniently defined via the in-plane current $\mathbf{j} = \partial\mathbf{P}/\partial t$. The current operator is obtained in the usual way from $\partial\mathcal{H}_\tau(\mathbf{k})/\partial\mathbf{k}$, where we retain only the leading terms at $k \rightarrow 0$:

$$\hat{\mathbf{j}}(\mathbf{r}) = ev \sum_{\tau} \hat{\psi}_{\tau}^{\dagger}(\mathbf{r}) \begin{bmatrix} 0 & \tau\mathbf{e}_x - i\mathbf{e}_y \\ \tau\mathbf{e}_x + i\mathbf{e}_y & 0 \end{bmatrix} \hat{\psi}_{\tau}(\mathbf{r}), \quad (11)$$

where $\mathbf{e}_x, \mathbf{e}_y$ are the unit vectors in the corresponding directions. Using the Kubo formula, whose general form

for the susceptibility $\chi_{\mathcal{A}\mathcal{B}}(\omega)$ determining the response of a quantity \mathcal{A} to the periodic force which couples to a quantity \mathcal{B} reads as

$$\chi_{\mathcal{A}\mathcal{B}}(\omega) = i \int_0^{\infty} \langle [\hat{\mathcal{A}}(t), \hat{\mathcal{B}}(0)] \rangle e^{i\omega t} dt,$$

where $\hat{\mathcal{A}}(t), \hat{\mathcal{B}}(0)$ are the time-dependent operators in the Heisenberg representation of the unperturbed Hamiltonian and the average is taken over the unperturbed equilibrium state, we obtain the following expression for the polarization susceptibility:

$$\chi_{\alpha\beta}(\mathbf{r}, \mathbf{r}', \omega) = \sum_{\nu} \frac{\langle 0 | \hat{j}_{\alpha}(\mathbf{r}) | \nu \rangle \langle \nu | \hat{j}_{\beta}(\mathbf{r}') | 0 \rangle}{E_{\nu}^2 (E_{\nu} - \omega - i0^+)}, \quad (12)$$

$$\chi_{\alpha z}(\mathbf{r}, \mathbf{r}', \omega) = i \sum_{\nu} \frac{\langle 0 | \hat{j}_{\alpha}(\mathbf{r}) | \nu \rangle \langle \nu | \hat{P}_z(\mathbf{r}') | 0 \rangle}{E_{\nu} (E_{\nu} - \omega - i0^+)}, \quad (13)$$

$$\chi_{zz}(\mathbf{r}, \mathbf{r}', \omega) = \sum_{\nu} \frac{\langle 0 | \hat{P}_z(\mathbf{r}) | \nu \rangle \langle \nu | \hat{P}_z(\mathbf{r}') | 0 \rangle}{E_{\nu} - \omega - i0^+}. \quad (14)$$

Here $|0\rangle$ and $|\nu\rangle$ are the ground and excited electronic states, E_{ν} is their energy difference (that is, the energy of the excitation ν), the indices $\alpha, \beta = x, y$, and we omitted the non-resonant terms. The infinitesimal imaginary part $i0^+$ in the denominators reflects the causal nature of the susceptibility and determines its analytical properties (the susceptibility must be analytical in the upper complex half-plane of ω). In the translationally invariant case, the susceptibilities depend only on the difference $\mathbf{r} - \mathbf{r}'$, so

$$\chi_{ij}(\mathbf{r} - \mathbf{r}', \omega) = \int \frac{d^2\mathbf{q}}{(2\pi)^2} e^{i\mathbf{q}\cdot(\mathbf{r}-\mathbf{r}')} \chi_{ij}(\mathbf{q}, \omega). \quad (15)$$

Here the in-plane components x, y are labeled by the Greek indices α, β , while the Latin indices run over all three dimensions, $i, j = x, y, z$.

In the following, we evaluate $\chi_{ij}(\mathbf{q}, \omega)$ using the eigenstates $|\nu\rangle$ which are the lowest-energy states of the intravalley excitons, whose spins are mixed by the Rashba coupling. The effect of the Zeeman coupling is treated analogously, the result is summarized in the end of Sec. III C.

B. Excitonic states

We start by constructing the zero-approximation states, i. e., those in the absence of the Rashba coupling. First, each intravalley exciton can be characterized by the index τ , indicating the valley in which the electronic transition takes place. It gives rise to two species of intravalley excitons, which can be distinguished by the valley index $\tau = \pm 1$. Further, in each valley the conduction and valence bands are spin split, so the excitonic states

can be labeled by a pair of spin indices $s_c, s_v = \uparrow, \downarrow$ referring to the conduction and the valence band, respectively (the hole spin is given by $-s_v$). Finally, the excitonic state is characterized by a center-of-mass momentum \mathbf{q} . So, the zero-approximation excitonic states are written as

$$|\tau, s_c, s_v, \mathbf{q}\rangle_0 = \int d^2\mathbf{r}_e d^2\mathbf{r}_h \frac{e^{i\mathbf{q}\mathbf{r}_{cm}}}{\sqrt{S}} \Phi(\mathbf{r}_e - \mathbf{r}_h) \times \hat{\psi}_{\tau, s_c, s_e}^\dagger(\mathbf{r}_e) \hat{\psi}_{\tau, s_v, s_v}(\mathbf{r}_h) |0\rangle. \quad (16)$$

Here, S is the sample area, \mathbf{r}_{cm} is the center-of-mass coordinate, $\mathbf{r}_{cm} \equiv (m_e\mathbf{r}_e + m_h\mathbf{r}_h)/(m_e + m_h)$, and $\Phi(\mathbf{r}_e - \mathbf{r}_h)$ is the normalized wave function of the relative electron-hole motion, corresponding to the lowest bound state, which was discussed in Sec. II B. States (16) are normalized as

$${}_0\langle \tau, s_c, s_v, \mathbf{q} | \tau', s'_c, s'_v, \mathbf{q}' \rangle_0 = \delta_{\tau\tau'} \delta_{s_c s'_c} \delta_{s_v s'_v} \delta_{\mathbf{q}\mathbf{q}'}, \quad (17)$$

and have the energies

$$E_{\tau, s_c, s_v}^{(0)}(\mathbf{q}) = E_g - E_b + \tau(s_c\Delta_c - s_v\Delta_v) + \frac{q^2}{2m_{ex}}, \quad (18)$$

where we introduced the excitonic mass $m_{ex} \equiv m_e + m_h$.

The Rashba coupling flips electron and hole spins and mixes the excitonic states with different s_c, s_v . As $\Delta_c/\Delta_v \sim 0.1 \ll 1$, we neglect the spin-flip in the valence band, and consider it only in the conduction band. It can be described by an effective 2×2 Hamiltonian in the basis of $\{|\tau, \uparrow, s_v, \mathbf{q}\rangle_0, |\tau, \downarrow, s_v, \mathbf{q}\rangle_0\}$, obtained by the projection of the electronic Rashba Hamiltonian (10) on the excitonic states:

$$\hat{H}_{\tau, s_v}^{ex}(\mathbf{q}) = \begin{bmatrix} E_{\tau, \uparrow, s_v}(\mathbf{q}) & -i\lambda_{ex}q_- \\ i\lambda_{ex}q_+ & E_{\tau, \downarrow, s_v}(\mathbf{q}) \end{bmatrix}, \quad (19)$$

where the excitonic Rashba coupling constant is given by

$$\lambda_{ex} = \frac{vd_z\mathcal{E}_z}{E_g} \frac{m_e}{m_e + m_h}. \quad (20)$$

Description of spin flip in terms of the purely excitonic effective Hamiltonian (19) assumes that the spin flip does not disturb the electron-hole relative motion inside the exciton, which is guaranteed by the condition $\Delta_c, \lambda_{ex}q \ll E_b$ [60].

The 2×2 Hamiltonian (19) can be diagonalized exactly; however, we are interested only in small momenta q , so perturbative expressions will suffice for us. Up to second order in λ_{ex} , the mixed-spin eigenstates are given by

$$|\tau, \uparrow, s_v, \mathbf{q}\rangle_{mix} = \frac{|\tau, \uparrow, s_v, \mathbf{q}\rangle_0}{1 + w_{\mathbf{q}}/2} + \frac{i\lambda_{ex}q_+}{2\tau\Delta_c} |\tau, \downarrow, s_v, \mathbf{q}\rangle_0, \quad (21)$$

$$|\tau, \downarrow, s_v, \mathbf{q}\rangle_{mix} = \frac{|\tau, \downarrow, s_v, \mathbf{q}\rangle_0}{1 + w_{\mathbf{q}}/2} + \frac{i\lambda_{ex}q_-}{2\tau\Delta_c} |\tau, \uparrow, s_v, \mathbf{q}\rangle_0, \quad (22)$$

where $w_{\mathbf{q}} \equiv \lambda_{ex}^2 q^2 / (4\Delta_c^2)$. To the same order, their energies are given by

$$E_{\tau, s_c, s_v}^{mix}(\mathbf{q}) = E_{\tau, s_c, s_v}^{(0)}(\mathbf{q}) + \tau s_c \frac{\lambda_{ex}^2}{2\Delta_c} q^2. \quad (23)$$

The states with $s_c = s_v = \uparrow$ from the \mathbf{K} valley and those with $s_c = s_v = \downarrow$ from the $-\mathbf{K}$ valley are called the bright A excitons. Those with the opposite s_c, s_v have a higher energy (due to the Δ_v term) and are called the bright B excitons. Their energies are

$$E_{A,B}^b(\mathbf{q}) = E_g - E_b + \frac{q^2}{2m_{ex}} \mp \Delta_v \pm \Delta_c \pm \frac{\lambda_{ex}^2}{2\Delta_c} q^2. \quad (24)$$

The states obtained by flipping the spin in the conduction band can be called the dark A and B excitons, their energies are [61]

$$E_{A,B}^d(\mathbf{q}) = E_{A,B}^b(\mathbf{q}) \mp 2 \left(\Delta_c + \frac{\lambda_{ex}^2}{2\Delta_c} q^2 \right). \quad (25)$$

C. Calculation of susceptibility

We calculate the susceptibility $\chi_{ij}(\mathbf{q}, \omega)$ from Eqs. (12)–(14) using the matrix elements $\langle 0 | \hat{j}_\alpha(\mathbf{r}) | \nu \rangle$ and $\langle 0 | \hat{P}_z(\mathbf{r}) | \nu \rangle$, which, in turn, are obtained from expressions (21) and (22) for the mixed-spin eigenstates $|\nu\rangle$ and from the matrix elements between the zero-approximation states (16) following from the definitions of the in-plane current and the z -dipole moment operators [Eqs. (11) and (8)]. Namely, for the in-plane current we have

$$\langle 0 | \hat{j}_\alpha(\mathbf{r}) | \tau, s_c, s_v, \mathbf{q} \rangle_0 = ev\Phi(0) \frac{e^{i\mathbf{q}\mathbf{r}}}{\sqrt{S}} (\tau\delta_{\alpha x} + i\delta_{\alpha y}) \delta_{s_c s_v}. \quad (26)$$

The nonzero matrix elements of the z -dipole moment operator between the ground state and the zero-approximation states are

$$\langle 0 | \hat{P}_z(\mathbf{r}) | 1, \downarrow, \uparrow, \mathbf{q} \rangle_0 = id_z \Phi(0) \frac{e^{i\mathbf{q}\mathbf{r}}}{\sqrt{S}}, \quad (27)$$

$$\langle 0 | \hat{P}_z(\mathbf{r}) | -1, \uparrow, \downarrow, \mathbf{q} \rangle_0 = id_z \Phi(0) \frac{e^{i\mathbf{q}\mathbf{r}}}{\sqrt{S}}. \quad (28)$$

Summation over $\tau = \pm 1$ in combination with the independence of the energies $E_{A,B}^{b,d}(\mathbf{q})$ on the valley index τ restores the in-plane isotropy in the final expressions for the susceptibility, written to the second order in d_z :

$$\chi_{\alpha\beta}(\mathbf{q}, \omega) = 2\delta_{\alpha\beta} \frac{[ev\Phi(0)]^2}{E_A^2} \left[\frac{1 - w_{\mathbf{q}}}{E_A^b(\mathbf{q}) - \omega} + \frac{w_{\mathbf{q}}}{E_A^d(\mathbf{q}) - \omega} \right] + 2\delta_{\alpha\beta} \frac{[ev\Phi(0)]^2}{E_B^2} \left[\frac{1 - w_{\mathbf{q}}}{E_B^b(\mathbf{q}) - \omega} + \frac{w_{\mathbf{q}}}{E_B^d(\mathbf{q}) - \omega} \right], \quad (29)$$

$$\chi_{z\alpha}(\mathbf{q}, \omega) = -\chi_{\alpha z}(\mathbf{q}, \omega) = i \frac{q_\alpha \lambda_{ex}}{\Delta_c} d_z \frac{ev\Phi^2(0)}{E_A} \left[\frac{1}{E_A^b(\mathbf{q}) - \omega} - \frac{1}{E_A^d(\mathbf{q}) - \omega} \right], \quad (30)$$

$$\chi_{zz}(\mathbf{q}, \omega) = 2d_z^2 \Phi^2(0) \frac{1}{E_A^d(\mathbf{q}) - \omega}. \quad (31)$$

Here we omitted the infinitesimal imaginary part in the denominator to keep the formulas more compact and approximated $E_{A,B}^{\text{b,d}}(\mathbf{q}) \approx E_{A,B}$ in the non-resonant prefactor, neglecting the dispersion and the conduction band splitting. Note also that $\Phi(0)$ is a real quantity.

From Eq. (29), we see the crucial role played by the quantity $w_{\mathbf{q}} \equiv \lambda_{\text{ex}}^2 q^2 / (4\Delta_c^2)$, introduced in Sec. III B. It represents the spectral weight transferred from the bright to the dark excitons by the Rashba coupling. Let us estimate its order of magnitude. Taking the numerical values typical of WSe₂, $cq = 1.7$ eV, the experimentally determined splitting $2\Delta_c = -30$ meV [31], and $\lambda_{\text{ex}} = 9$ meV·Å from [46] for a quite strong perpendicular electric field $\mathcal{E}_z = 0.1$ V/Å, we still obtain a very small value of $w_{\mathbf{q}} \approx 0.7 \times 10^{-7}$.

If instead of the perpendicular electric field \mathcal{E}_z , an in-plane magnetic field B_{\parallel} is applied, spin mixing due to the Zeeman effect can be taken into account by full analogy with the Rashba mixing. In fact, it is sufficient to replace $\lambda_{\text{ex}} q \rightarrow |g_c \mu_B B_{\parallel}|/2$, so Eq. (30) has the same form, but the transferred spectral weight $w_{\mathbf{q}} = (g_c \mu_B B_{\parallel})^2 / (16\Delta_c^2)$. For a magnetic field $B_{\parallel} = 10$ T, we obtain a numerical estimate $w_{\mathbf{q}} \approx 4 \times 10^{-4}$. The in-plane direction of the off-diagonal component $\chi_{\alpha z}$ is determined not by \mathbf{q} , but by the magnetic field, $\chi_{\alpha z} \propto B_{\parallel\alpha}$.

IV. EXCITON RADIATIVE SHIFTS AND DECAY RATES

A. General scheme

Here we consider the interaction of excitons in the TMDC monolayer with the electromagnetic field. The monolayer is assumed to be sandwiched between two semi-infinite media with dielectric constants ε_1 and ε_2 occupying the half-spaces with $z > 0$ and $z < 0$, respectively. (Note that the values of $\varepsilon_{1,2}$ at optical frequencies $\sim E_A$ should be taken.) The free field in such a structure is fully characterized by the Green's function $D_{ij}(z, z'; \mathbf{q}, \omega)$, which represents the response of the electric field, $\mathcal{E}_i(z) e^{i\mathbf{q}\mathbf{r} - i\omega t}$, to an external oscillating polarization $P_j \delta(z - z') e^{i\mathbf{q}\mathbf{r} - i\omega t}$, located in the plane $z = z'$. In the quantum theory, this Green's function represents the retarded propagator of the electric field; at the same time, it can be found from the classical Maxwell equations [62]. The radiative self-energy for the excitons at $z = 0$ is proportional to $D_{ij}(0, 0; \mathbf{q}, \omega)$, for which we introduce the short-hand notation $\bar{D}_{ij}(\mathbf{q}, \omega)$ [more precisely, it represents the projection on the spatial profile of the excitonic polarization in the z -direction, here assumed to be just $\delta(z)$].

The long-range exchange part of the Coulomb interaction shifts the exciton energies and lifts the valley degeneracy. Exciton coupling to the photons also shifts the excitonic frequencies and leads to the radiative decay. All these effects can be described by studying the linear

system

$$P_i = \chi_{ij}(\mathbf{q}, \omega) \bar{D}_{jk}(\mathbf{q}, \omega) P_k. \quad (32)$$

For each \mathbf{q} , it has non-trivial solutions for some complex values of ω whose real parts give the shifted exciton energies, and the imaginary parts (with the opposite sign and multiplied by 2) represent the radiative decay rates. This procedure is equivalent to finding the poles of the full layer susceptibility (i. e., dressed by the exchange interaction and coupling to photons) in the complex plane of ω , or to finding the poles of the monolayer reflectivity.

Calculation of $\bar{D}_{ij}(\mathbf{q}, \omega)$ from the Maxwell equations is quite standard and is given in Appendix D. The result is

$$\begin{aligned} \bar{D}_{\alpha\beta}(\mathbf{q}, \omega) = & \left(\delta_{\alpha\beta} - \frac{q_{\alpha} q_{\beta}}{q^2} \right) \frac{4\pi i \omega^2 / c^2}{q_{1z} + q_{2z}} + \\ & + \frac{q_{\alpha} q_{\beta}}{q^2} \frac{4\pi i (q_{1z}/\varepsilon_1)(q_{2z}/\varepsilon_2)}{q_{1z}/\varepsilon_1 + q_{2z}/\varepsilon_2}, \end{aligned} \quad (33)$$

$$\begin{aligned} \bar{D}_{z\alpha}(\mathbf{q}, \omega) = & -\bar{D}_{\alpha z}(\mathbf{q}, \omega) = \\ = & 2\pi i q_{\alpha} \frac{q_{1z}/\varepsilon_1 - q_{2z}/\varepsilon_2}{q_{1z}/\varepsilon_1 + q_{2z}/\varepsilon_2}, \end{aligned} \quad (34)$$

$$\bar{D}_{zz}(\mathbf{q}, \omega) = \frac{4\pi i q^2}{q_{1z}/\varepsilon_1 + q_{2z}/\varepsilon_2} - 2\pi \kappa_0. \quad (35)$$

Here q_{1z} and q_{2z} are the z components of the three-dimensional wave vector in the corresponding media:

$$q_{1z,2z}(\mathbf{q}, \omega) = \sqrt{\varepsilon_{1,2}(\omega + i0^+)^2 / c^2 - q^2}, \quad (36)$$

where the infinitesimal imaginary part fixes the rule for the analytical continuation of the square root in the upper complex half-plane of ω , inherited from the analyticity of the response function $\bar{D}_{ij}(\mathbf{q}, \omega)$ in the upper half-plane. This prescribes $\text{Im } q_{1z,2z} > 0$ for real ω in the interval $|\omega| < cq/\sqrt{\varepsilon_{1,2}}$, which corresponds to evanescent waves. The parameter κ_0 in Eq. (35) represents the electric field of a double layer, arising from the excitonic polarization in the z direction (Appendix D), which is singular in the limit of an infinitely thin layer, and cannot be determined in the macroscopic framework, used here. For excitons in semiconductor quantum wells of a sizable width, this local-field effect could be treated properly in the envelope-function approximation [38, 49]. In the atomically-thin TMDC monolayer, it requires the full microscopic treatment of the short-range exchange interaction, such as that in [47]. The consequences of this local-field effect will be discussed in the next subsection.

The tensor structure of $\chi_{ij}(\mathbf{q}, \omega)$ and $\bar{D}_{jk}(\mathbf{q}, \omega)$, following from the in-plane isotropy of the problem, determines how the two-fold valley degeneracy of the mechanical excitons is lifted. The first family of solutions of Eq. (32) is characterized by \mathbf{P} lying in the xy plane, perpendicular to \mathbf{q} . These transverse excitons emit s -polarized light (transverse-electric, or TE modes). The second family of solutions has \mathbf{P} in the plane formed by the vectors \mathbf{q} and \mathbf{e}_z ; its precise direction is determined by the

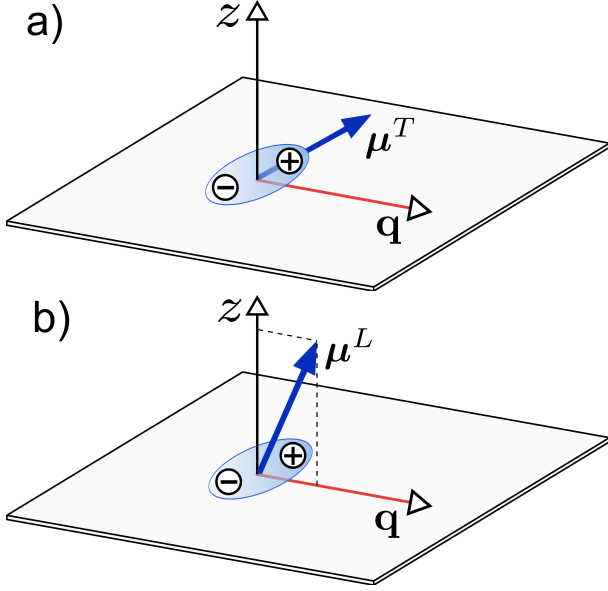


FIG. 3. Orientation of the transition dipole moments μ_ν^T , μ_ν^L of the transverse (a) and longitudinal (b) excitons with respect to the crystal plane, the z axis and the exciton momentum \mathbf{q} .

relative magnitude of different components of $\chi_{ij}(\mathbf{q}, \omega)$. These are longitudinal excitons, which emit p -polarized light (transverse-magnetic, or TM modes). Each of the two linear polarizations represents a linear combination of the two circularly polarized excitons from each valley with equal probability weights. In the following, we treat Eq. (32) perturbatively. Namely, we assume ω to be close to one of the poles E_ν of $\chi_{ij}(\mathbf{q}, \omega)$. Near the pole, it can be represented as

$$\chi_{ij}(\mathbf{q}, \omega) \approx \frac{\mu_{\nu i}^T (\mu_{\nu j}^T)^* + \mu_{\nu i}^L (\mu_{\nu j}^L)^*}{E_\nu - \omega}, \quad (37)$$

with some vectors μ_ν^T , μ_ν^L , which describe the polarization of the transverse and longitudinal excitons. The relative orientation of μ_ν^T , μ_ν^L with respect to the exciton momentum \mathbf{q} and the z axis is shown in Fig. 3.

Then, the corresponding solutions of Eq. (32) are $\mathbf{P} \propto \mu_\nu^T$ and $\mathbf{P} \propto \mu_\nu^L$, and the shifted (complex) excitonic energies are approximately given by

$$\begin{aligned} \tilde{E}_\nu^{T,L} &= E_\nu - (\mu_{\nu i}^{T,L})^* \bar{D}_{ij}(\mathbf{q}, E_\nu) \mu_{\nu j}^{T,L} \equiv \\ &\equiv E_\nu + \Omega_\nu - \frac{i\Gamma_\nu}{2}. \end{aligned} \quad (38)$$

Here, $-(\mu_{\nu i}^{T,L})^* \bar{D}_{ij}(\mathbf{q}, E_\nu) \mu_{\nu j}^{T,L}$ is nothing but the radiative self-energy of the exciton, in which we explicitly separate the radiative shift Ω_ν and the decay rate Γ_ν . This procedure is equivalent to the quantum-mechanical calculation of the energy shift by perturbation theory to the first order in the Coulomb exchange and to the second order in the exciton-photon coupling, and to the calculation of the radiative decay rate by the Fermi Golden Rule.

If the spin mixing is due to the Zeeman effect in an in-plane magnetic field \mathbf{B}_\parallel instead of the Rashba effect, the s and p polarizations do not separate, as \mathbf{q} and \mathbf{B}_\parallel define two different directions in the plane. We discuss this situation in Appendix E.

B. Momentum-dependent radiative shifts and decay rates

For the transverse bright and dark A excitons, the radiative shift and decay rate are straightforwardly evaluated as

$$\Omega_{TA}^{\text{b,d}}(\mathbf{q}) - \frac{i}{2} \Gamma_{TA}^{\text{b,d}}(\mathbf{q}) = \left\{ \begin{array}{l} 1 - w_{\mathbf{q}} \\ w_{\mathbf{q}} \end{array} \right\} \frac{8\pi}{i} \frac{(e^2/c)v^2\Phi^2(0)}{cq_{1z}^A + cq_{2z}^A}, \quad (39)$$

where the upper/lower line in the braces with $w_{\mathbf{q}} \equiv |\lambda_{\text{ex}}|^2 q^2 / (4\Delta_c^2)$ refers to the bright/dark exciton, and the expression to the right of the braces is the decay rate of the transverse bright A exciton in the absence of spin flip [40–43]. In the square roots, $q_{1z,2z}^A = \sqrt{\varepsilon_{1,2} E_A^2 / c^2 - q^2}$, we neglected the small difference between E_A^{b} and E_A^{d} as well as their dependence on \mathbf{q} , since we are interested only in a narrow region $q < \max\{\sqrt{\varepsilon_1}, \sqrt{\varepsilon_2}\} E_A / c$ where at least one of q_{1z}, q_{2z} is real [63, 64]. For the longitudinal A excitons we obtain more bulky expressions,

$$\begin{aligned} \Omega_{LA}^{\text{b}}(\mathbf{q}) - \frac{i}{2} \Gamma_{LA}^{\text{b}}(\mathbf{q}) &= -\frac{8\pi i \Phi^2(0)}{q_{1z}^A/\varepsilon_1 + q_{2z}^A/\varepsilon_2} \frac{e^2 v^2}{E_A^2} \frac{q_{1z}^A q_{2z}^A}{\varepsilon_1 \varepsilon_2} - \\ &- \frac{8\pi q^2 \Phi^2(0)}{q_{1z}^A/\varepsilon_1 + q_{2z}^A/\varepsilon_2} \frac{ev}{E_A} \frac{\lambda_{\text{ex}}}{2\Delta_c} \times \\ &\times \left[\left(\frac{q_{1z}^A}{\varepsilon_1} - \frac{q_{2z}^A}{\varepsilon_2} \right) d_z - i \frac{ev}{E_A} \frac{\lambda_{\text{ex}}}{2\Delta_c} \frac{q_{1z}^A q_{2z}^A}{\varepsilon_1 \varepsilon_2} \right], \end{aligned} \quad (40)$$

$$\begin{aligned} \Omega_{LA}^{\text{d}}(\mathbf{q}) - \frac{i}{2} \Gamma_{LA}^{\text{d}}(\mathbf{q}) &= -\frac{8\pi i q^2 \Phi^2(0)}{q_{1z}^A/\varepsilon_1 + q_{2z}^A/\varepsilon_2} \times \\ &\times \left[\frac{e^2 v^2}{E_A^2} \frac{\lambda_{\text{ex}}^2}{4\Delta_c^2} \frac{q_{1z}^A q_{2z}^A}{\varepsilon_1 \varepsilon_2} + d_z^2 \right] + \\ &+ \frac{8\pi q^2 \Phi^2(0)}{q_{1z}^A/\varepsilon_1 + q_{2z}^A/\varepsilon_2} \frac{ev}{E_A} \frac{\lambda_{\text{ex}}}{2\Delta_c} \left(\frac{q_{1z}^A}{\varepsilon_1} - \frac{q_{2z}^A}{\varepsilon_2} \right) d_z + \\ &+ 4\pi \kappa_0 d_z^2 \Phi^2(0). \end{aligned} \quad (41)$$

whose qualitative features are similar to the transverse case: the decay rates are nonzero only in the small-momentum region $q < \max\{\sqrt{\varepsilon_1}, \sqrt{\varepsilon_2}\} E_A / c$, the bright exciton radiative rate is dominated by the first line of Eq. (40) to which the Rashba term gives a small correction. However, an important difference from the transverse case is that Γ_{LA}^{d} does not vanish for $\lambda_{\text{ex}} = 0$. The longitudinal dark A exciton can decay even in the absence of the Rashba coupling, due to d_z . Moreover, this latter mechanism is by far the dominant one, as the ratio between the two terms in the square brackets of (41) is $\sim 10^{-5}$ for a quite high electric field of $\mathcal{E}_z = 0.1 \text{ V/\AA}$. Another important difference from the transverse case is

that far in the non-radiative zone, $q \gg \sqrt{\varepsilon_{1,2}}E_A/c$, the longitudinal exciton energies $\Omega_{LA}^{b,d}(\mathbf{q}) \propto q$. This is the effect of the exchange interaction, which was discussed in [65] (in that work, the intravalley part of the exchange interaction was not taken into account, which was later corrected in [41, 66]).

The last term in Eq. (41) containing the unknown parameter κ_0 is purely real and does not contribute to the radiative decay rate. However, it produces an energy shift,

$$\Xi_0 = 4\pi\kappa_0 d_z^2 \Phi^2(0), \quad (42)$$

of the longitudinal excitons, which thus lifts the valley degeneracy even at $\mathbf{q} = 0$ and in the absence of Rashba or Zeeman effects [67]. In the macroscopic framework, used here, Ξ_0 represents the interaction energy of the exciton polarization in the z direction with its own electric field, which is singular in the limit of an infinitely thin layer. By the order of magnitude, $\kappa_0 \sim \varepsilon/d$, where d is the monolayer thickness and $\varepsilon \approx 7$ is the effective background dielectric constant in the perpendicular direction at optical frequencies (see Appendix D). Taking $d = 3 \text{ \AA}$, $\varepsilon = 3$, $d_z/e = 0.08 \text{ \AA}$, and $\Phi(0) \sim 0.1 \text{ \AA}^{-1}$, we obtain an estimate $\Xi_0 \sim 10 \text{ meV}$. This value agrees by the order of magnitude with the dark exciton energy shifts due to the short-range exchange interaction, which were calculated using a microscopic *ab initio* approach in [47]. Indeed, both are supposed to have the same origin, as the Coulomb part of $\bar{D}_{ij}(\mathbf{q}, \omega)$ represents the exchange field. However, no lifting of valley degeneracy was mentioned in [47]. Note that the presence of the positive shift Ξ_0 for the longitudinal excitons has an important consequence for the luminescence, as the lowest-energy states are the transverse excitons whose decay rate is only due to Rashba or Zeeman effect.

To illustrate the q dependence of the radiative energy shifts and the decay rates, we plot them in Figs. 4 and 5 for the transverse and longitudinal dark A excitons, for $\varepsilon_1 = 1$ and two values of the substrate dielectric constant, one typical for glass-like substrates, $\varepsilon_2 = 2.4$, the other one corresponding to a highly dielectric substrate, such as AlGaSb with $\varepsilon_2 = 25$ at optical frequencies [68]. It is convenient to normalize the energy shifts and decay rates by the bright exciton decay rate at $\mathbf{q} = 0$, $\Gamma_{TA}^b(0) = \Gamma_{LA}^b(0) \equiv \Gamma_0$, for a TMDC monolayer suspended in vacuum,

$$\Gamma_0 = 8\pi \frac{e^2}{c} \frac{v^2 \Phi^2(0)}{E_A}. \quad (43)$$

For $v = 2.6 \text{ eV} \cdot \text{\AA}$, $E_A = 1.7 \text{ eV}$, $\Phi(0) = 0.1 \text{ \AA}^{-1}$, this estimate gives $\Gamma_0 \approx 7 \text{ meV} \approx (100 \text{ fs})^{-1}$, not very much different from the results of more precise calculations involving the full microscopic treatment of the exciton wave function [42, 43], which give $1/\Gamma_0 \approx 200 \text{ fs}$ for several TMDC materials. In the calculation presented in Figs. 4,5, we used the values $E_A = 1.7 \text{ eV}$, the experimentally determined splitting $2\Delta_c = -30 \text{ meV}$ [31], $d_z/e = 0.08 \text{ \AA}$ as

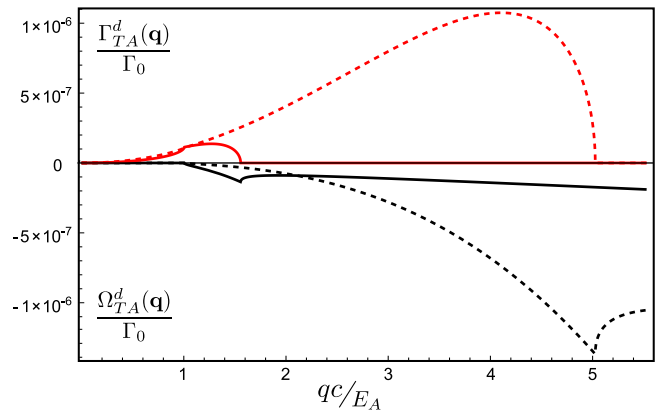


FIG. 4. The normalized radiative energy shifts $\Omega_{TA}^d(\mathbf{q})/\Gamma_0$ (black curves, negative y axis) and decay rates $\Gamma_{TA}^d(\mathbf{q})/\Gamma_0$ (red curves, positive y axis) of transverse excitons for $\varepsilon_1 = 1$, $\varepsilon = 2.4$ (solid curves) and $\varepsilon = 25$ (dashed curves), as a function of the dimensionless exciton momentum qc/E_A .

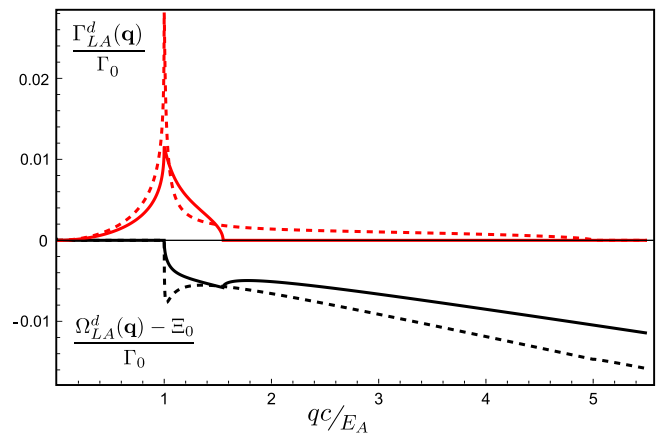


FIG. 5. The normalized radiative energy shifts (excluding the short-range exchange splitting Ξ_0) $[\Omega_{LA}^d(\mathbf{q}) - \Xi_0]/\Gamma_0$ (black curves, negative y axis) and decay rates $\Gamma_{LA}^d(\mathbf{q})/\Gamma_0$ (red curves, positive y axis) of longitudinal excitons for $\varepsilon_1 = 1$, $\varepsilon = 2.4$ (solid curves) and $\varepsilon = 25$ (dashed curves), as a function of the dimensionless exciton momentum qc/E_A .

extracted from [46], and the Rashba coupling constant $\lambda_{\text{ex}} = 90 \text{ meV} \cdot \text{\AA}$ per each V/\AA of the static electric field \mathcal{E}_z [46]. The latter was taken to be 0.1 V/\AA for the glass-like substrate, giving $\lambda_{\text{ex}} = 9 \text{ meV} \cdot \text{\AA}$, and 0.2 eV/\AA for the highly dielectric substrate ($\lambda_{\text{ex}} = 18 \text{ meV} \cdot \text{\AA}$), as estimated in Appendix C (note that changing the electric field amounts to a simple rescaling of the y axis $\propto \mathcal{E}_z^2$ in Fig. 4, while Fig. 5 is insensitive to \mathcal{E}_z , as discussed above).

C. Integrated decay rates

So far, we calculated the decay rates $\Gamma_\nu(\mathbf{q})$ for the excitonic states with a given momentum \mathbf{q} and these rates depend quite strongly on q . It is interesting to compare

the overall efficiency of different decay mechanisms, studied here, with respect to the radiative decay of bright excitons. To do this, we integrate the obtained decay rates over \mathbf{q} . For bright excitons, integration of Eqs. (39) and (40) gives

$$\int \frac{d^2\mathbf{q}}{(2\pi)^2} \frac{\Gamma_{TA}^b(\mathbf{q}) + \Gamma_{LA}^b(\mathbf{q})}{\Gamma_0} = \frac{E_A^2}{2\pi c^2} 2\mathcal{F}_b(\varepsilon_1, \varepsilon_2), \quad (44)$$

where $\mathcal{F}_b(\varepsilon_1, \varepsilon_2)$ is a function of the two dielectric constants, whose explicit form is given in Appendix F. For dark exciton decay due to the Rashba spin-orbit coupling, we integrate Eqs. (39) and (41) and obtain

$$\int \frac{d^2\mathbf{q}}{(2\pi)^2} \frac{\Gamma_{LA}^d(\mathbf{q})}{\Gamma_0} = \frac{E_A^2}{2\pi c^2} \eta_{d_z} \mathcal{F}_d^L(\varepsilon_1, \varepsilon_2), \quad (45)$$

$$\int \frac{d^2\mathbf{q}}{(2\pi)^2} \frac{\Gamma_{TA}^d(\mathbf{q})}{\Gamma_0} = \frac{E_A^2}{2\pi c^2} \eta_R \mathcal{F}_T^d(\varepsilon_1, \varepsilon_2), \quad (46)$$

while in the presence of the in-plane Zeeman field we integrate Eqs. (E6), (E7) of Appendix E:

$$\int \frac{d^2\mathbf{q}}{(2\pi)^2} \frac{\Gamma_{\parallel}^d(\mathbf{q})}{\Gamma_0} = \frac{E_A^2}{2\pi c^2} [\eta_{d_z} \mathcal{F}_d^L(\varepsilon_1, \varepsilon_2) + \eta_Z \mathcal{F}_b(\varepsilon_1, \varepsilon_2)], \quad (47)$$

$$\int \frac{d^2\mathbf{q}}{(2\pi)^2} \frac{\Gamma_{\perp}^d(\mathbf{q})}{\Gamma_0} = \frac{E_A^2}{2\pi c^2} \eta_Z \mathcal{F}_b(\varepsilon_1, \varepsilon_2). \quad (48)$$

The explicit form of the functions $\mathcal{F}_T^d(\varepsilon_1, \varepsilon_2)$, $\mathcal{F}_d^L(\varepsilon_1, \varepsilon_2)$, $\mathcal{F}_b(\varepsilon_1, \varepsilon_2)$ is given in Appendix F. For $\varepsilon_1 = 1$, $\varepsilon_2 = 2.4$, they are equal to 1.5, 1.6, and 1.0, respectively. The factors η_{d_z} , η_R and η_Z are defined as

$$\eta_{d_z} = \frac{d_z^2}{e^2} \left(\frac{E_A}{v} \right)^2, \quad (49)$$

$$\eta_R = \frac{\lambda_{\text{ex}}^2}{4\Delta_c^2} \left(\frac{E_A}{c} \right)^2, \quad (50)$$

$$\eta_Z = \left(\frac{g_{\parallel} \mu_B B_{\parallel}}{4\Delta_c} \right)^2. \quad (51)$$

Their values are estimated to be $\eta_{d_z} \approx 3 \times 10^{-3}$, $\eta_R \approx 0.7 \times 10^{-7}$ for the perpendicular electric field $\mathcal{E}_z = 0.1\text{V}/\text{\AA}$, and $\eta_Z \approx 4 \times 10^{-3}$ for the in-plane magnetic field $B_{\parallel} = 30\text{ T}$ and $g_{\parallel} = -2$. These estimates represent the main result of the present paper. Indeed, since all $\mathcal{F}^{b,d}(\varepsilon_1, \varepsilon_2) \sim 1$, the relative importance of different decay mechanisms is mainly determined by the factors η_R , η_{d_z} , and η_Z .

The momentum-integrated decay rates, calculated above, besides giving a simple estimate of relative importance of each decay mechanism, also determine the total oscillator strength of each exciton species, which plays a role in different physical situations. One such situation is a disordered sample, where exciton center-of-mass motion is no longer free, so its wave function is not a plane wave $e^{i\mathbf{q}\mathbf{r}}$. If, instead, the exciton state has

some complicated center-of-mass wave function $\Psi(\mathbf{r})$, its decay rate is determined by the weights $|\langle \mathbf{q} | \Psi \rangle|^2$ of different plane waves in this state (here we use the fact that the exciton-photon coupling is diagonal in the in-plane momentum \mathbf{q}):

$$\Gamma[\Psi] = \int \frac{d^2\mathbf{q}}{(2\pi)^2} \Gamma(\mathbf{q}) |\langle \mathbf{q} | \Psi \rangle|^2. \quad (52)$$

If the characteristic spatial scale of $\Psi(\mathbf{r})$ (mean free path or localization length) is shorter than the light wavelength $2\pi c/E_A$, one can approximate $|\langle \mathbf{q} | \Psi \rangle|^2$ by a constant in the narrow radiative region, and then the decay rate is determined by the momentum integral of $\Gamma(\mathbf{q})$.

Another context in which the integral of $\Gamma(\mathbf{q})$ arises, is the thermal average [39]. Indeed, if the excitons have the Maxwell-Boltzmann momentum distribution, $f(\mathbf{q}) \propto e^{-q^2/(2m_{\text{ex}}T)}$, where T is the temperature and $m_{\text{ex}} = m_e + m_h$ is the exciton mass, the typical thermal momenta $q \sim \sqrt{m_{\text{ex}}T}$ are usually much larger than the radiative momentum E_A/c . Then, the thermal average can be approximated as

$$\begin{aligned} \langle \Gamma_A \rangle &= \sum_{\nu} \int \frac{d^2\mathbf{q}}{(2\pi)^2} \frac{f_{\nu}(\mathbf{q})}{n_{\text{ex}}} \Gamma_{\nu}(\mathbf{q}) \approx \\ &\approx \sum_{\nu} \frac{f_{\nu}(0)}{n_{\text{ex}}} \int \frac{d^2\mathbf{q}}{(2\pi)^2} \Gamma_{\nu}(\mathbf{q}), \end{aligned} \quad (53)$$

where the summation is over the four species of A excitons (two bright and two dark), and n_{ex} is their total density. Such average would represent the global radiative decay rate of the whole thermal excitonic population, and the relative contribution of each exciton species would correspond to the relative intensity of luminescence from each species. It is in this context that the difference between MoX_2 and WX_2 becomes important: while the calculation of $\Gamma_{\nu}(\mathbf{q})$ in Sec. (IV B) was equally applicable to both cases, the lower energy of the dark excitons in tungsten-based compounds results in a larger weight of dark excitons in the luminescence. Namely, the weight of the bright excitons is small by a factor $e^{-2\Delta_c/T}$. Similarly, the contribution of longitudinal dark excitons is small by a factor $e^{-\Xi_0/T}$ with respect to the transverse contribution.

It should be noted, however, that the equilibrium average (53) is based on the assumption of the exciton thermalization in the radiative region. This requires the thermalization rate to be larger than the radiative rate, in order to quickly supply the excitons into the narrow radiative region with small $q \sim E_A/c$. This is not always the case; for example, the full kinetic treatment of excitons interacting with acoustic phonons in GaAs quantum wells revealed a relaxation bottleneck at the border of the radiative region [69]. To check, whether the excitons in the radiative region are thermalized, one should compare the radiative rate $\Gamma(\mathbf{q})$ with the acoustic phonon absorption rate $1/\tau_0$ [70]. For TMDCs, $1/\tau_0 = aT$, where for the constant a values of a few tens of $\mu\text{eV}/K$ have

been reported [71–75], which is much longer than the sub-picosecond radiative rate for the bright excitons [42, 43] at temperatures lower than about 100 K. At lower temperatures, the bright exciton distribution in the radiative region is thus expected to be different from the thermal one. At the same time, for dark excitons whose radiative decay is at least 100 times slower than for the bright ones (see Fig. 5), so the thermal approximation should work reasonably well.

V. CONCLUSIONS AND OUTLOOK

In this work we have investigated the radiative decay of spin-forbidden dark intravalley A excitons in tungsten dichalcogenide monolayers due to several spin-flip mechanisms. Our main result is represented by expressions (49)–(51) for the average efficiencies η_R , η_z , and η_Z of different spin-flip mechanisms with respect to the main radiative decay mechanism of the bright excitons. As the bright excitons in tungsten-based compounds have higher energy than the dark ones, the bright exciton contribution to the photoluminescence is suppressed at low temperatures by the thermal activation exponential $e^{-2\Delta_c/T}$ with the bright-dark splitting $2\Delta_c$ of several tens of meV, of the order of the room temperature.

The intrinsic mechanism of the dark exciton radiative decay is due to the interband spin-flip dipole moment, perpendicular to the monolayer plane. It was mentioned in [40, 47], and its magnitude can be deduced from the estimates of [46]. We found, however, that the very same mechanism lifts the valley degeneracy of the dark excitons by a Coulomb local-field effect, producing a splitting Ξ_0 which we could very roughly estimate as about 10 meV. Crucially, the whole oscillator strength of such interband spin flip (about $\eta_z \sim 10^{-2} - 10^{-3}$ of the bright exciton oscillator strength) is taken by the higher-energy component. Thus, the spin-forbidden intravalley exciton, usually referred to as dark, in fact, has two components, one dark and the other which can be called “dim”. The contribution of this dim exciton to the photoluminescence is exponentially suppressed at low temperatures, $e^{-\Xi_0/T}$.

For the lowest-energy dark component, which should dominate the exciton population at low temperatures, we have analyzed extrinsic spin-flip mechanisms, which transfer some oscillator strength from the bright exciton to the dark one. One such mechanism is due to the Rashba spin-orbit coupling which arises whenever the reflection symmetry in the monolayer plane is broken, e. g., by an externally applied perpendicular static electric field, or by different dielectric environment above and below the monolayer. This mechanism was mentioned in [45]. Using our own estimate of 0.1 V/\AA for the effective electric field produced by the dielectric mismatch and the calculated value of the Rashba coupling constant from [46], we find that the fraction of the oscillator strength transferred from the bright exciton to the dark one is extremely low, about $\eta_R \sim 10^{-7}$, mainly due to small

momenta of excitons subject to radiative decay. Another possible mechanism is the spin flip by the Zeeman effect from a magnetic field directed along the monolayer plane. Then, for a strong but still realistic field of 30 T, a fraction $\eta_Z > 10^{-3}$ of the bright exciton oscillator strength can be transferred to the dark one. This suggests a way to manipulate the radiative properties of dark excitons.

The results of the present work help to identify several directions for improvement of our understanding of the excitonic radiative processes in tungsten dichalcogenides. First, the value of the interband spin-flip dipole moment is currently known from only one source, the estimate of [46]. It would be quite helpful if more information were available, either theoretically or experimentally. e. g., by studying the effect of the Rashba spin-orbit coupling on the carrier transport, as the Rashba coupling has the same origin. Second, a reliable microscopic calculation of the dark-dim exciton splitting Ξ_0 would help to determine how dramatic is the low-temperature suppression of the dim exciton population. Finally, the role of collisions with defects, charge carriers, or phonons in the radiative decay also needs clarification.

VI. ACKNOWLEDGEMENTS

We are grateful to M. Potemski for stimulating discussions. A. O. S. acknowledges financial support from the EC Graphene Flagship project (No. 604391).

Appendix A: Interband spin-flip dipole matrix element

To fix the form of d_z in Eq. (8), let us start from the Bloch states of TMDC monolayer obtained without taking into account the spin-orbit coupling. The construction involves the top valence band (v), the lowest conduction band (c), and a third band (z), which we take to be the next highest conduction band [46]. The coordinate wave functions of the corresponding states at $\pm\mathbf{K}$ points can be written as $u_{v,\pm\mathbf{K}}(\mathbf{r}) e^{\pm i\mathbf{K}\mathbf{r}}$, $u_{c,\pm\mathbf{K}}(\mathbf{r}) e^{\pm i\mathbf{K}\mathbf{r}}$, $u_{z,\pm\mathbf{K}}(\mathbf{r}) e^{\pm i\mathbf{K}\mathbf{r}}$. With respect to the reflection $z \rightarrow -z$ in the crystal plane, the functions $u_{v,\pm\mathbf{K}}$ and $u_{c,\pm\mathbf{K}}$ are even, while $u_{z,\pm\mathbf{K}}$ is odd. Time reversal symmetry of the Hamiltonian without the spin-orbit coupling imposes

$$u_{z,-\mathbf{K}} = e^{i\varphi_z} u_{z,\mathbf{K}}^*, \quad (\text{A1})$$

$$u_{c,-\mathbf{K}} = e^{i\varphi_c} u_{c,\mathbf{K}}^*, \quad (\text{A2})$$

$$u_{v,-\mathbf{K}} = e^{i\varphi_v} u_{v,\mathbf{K}}^*, \quad (\text{A3})$$

where u^* denotes the complex conjugate of u and $\varphi_{v,c,z}$ are some phases which we can choose freely. At the same time, reflection symmetry $x \rightarrow -x$ requires

$$u_{z,-\mathbf{K}} = e^{i\phi_z} \bar{u}_{z,\mathbf{K}}, \quad (\text{A4})$$

$$u_{c,-\mathbf{K}} = e^{i\phi_c} \bar{u}_{c,\mathbf{K}}, \quad (\text{A5})$$

$$u_{v,-\mathbf{K}} = e^{i\phi_v} \bar{u}_{v,\mathbf{K}}, \quad (\text{A6})$$

where we denote $\bar{u}(x, y, z) = u(-x, y, z)$, and $\phi_{v,c,z}$ are some other phases. One can choose either the φ phases or the ϕ phases, but as soon as one set is fixed, the other one is fixed too. The requirement for the $\mathbf{k} \cdot \mathbf{p}$ perturbation theory to give a Dirac-like coupling between the valence and the conduction band with a real velocity (v in Eq. 3) translates into the following condition:

$$\langle u_{c,\pm\mathbf{K}} | (-i\hbar\nabla/m) | u_{v,\pm\mathbf{K}} \rangle = v(\pm\mathbf{e}_x - i\mathbf{e}_y), \quad (\text{A7})$$

where the bracket notations stand for the integration in the coordinate space:

$$\langle u_1 | \hat{O} | u_2 \rangle \equiv \int u_1^*(\mathbf{r}) \hat{O} u_2(\mathbf{r}) d^3\mathbf{r}. \quad (\text{A8})$$

Condition (A7) fixes $\varphi_c = \varphi_v$, $\phi_c = \phi_v$.

The spin structure is described by the two spinors

$$\chi_\uparrow = \begin{pmatrix} 1 \\ 0 \end{pmatrix}, \quad \chi_\downarrow = \begin{pmatrix} 0 \\ 1 \end{pmatrix},$$

so the full wave functions in each band become $u_{\pm\mathbf{K}}(\mathbf{r}) e^{\pm i\mathbf{K}\mathbf{r}} \chi_\uparrow$, $u_{\pm\mathbf{K}}(\mathbf{r}) e^{\pm i\mathbf{K}\mathbf{r}} \chi_\downarrow$. The Zeeman term is $g\mu_B \mathbf{B} \cdot \boldsymbol{\sigma}/2$, where the Pauli matrices act on the spinors. The spin-orbit coupling introduces the spin splitting terms $\pm\Delta_{v,c}\sigma_z$ for the valence/conduction band at the $\pm\mathbf{K}$ point. When both $\Delta_{v,c} > 0$, the top valence band wave function at the \mathbf{K} point is $u_{v,\mathbf{K}} e^{i\mathbf{K}\mathbf{r}} \chi_\uparrow$, and the bottom conduction band wave function is $u_{c,\mathbf{K}} e^{i\mathbf{K}\mathbf{r}} \chi_\downarrow$, so the optical transition requires a spin flip.

The spin-flip transition dipole moment d_z is constructed from the second-order perturbation theory involving a virtual transition to the band (z), once with the z operator, and once with the spin-orbit coupling $\propto \hat{L}_+\sigma_- + \hat{L}_-\sigma_+$, where $\hat{L}_\pm = \hat{L}_x \pm i\hat{L}_y$. Denoting the corresponding matrix element in the respective valleys by $d_{\pm\mathbf{K}}$, we can write (up to constant factors)

$$d_{\pm\mathbf{K}} \sim \langle u_{v,\pm\mathbf{K}} | z | u_{z,\pm\mathbf{K}} \rangle \langle u_{z,\pm\mathbf{K}} | \hat{L}_\mp | u_{c,\pm\mathbf{K}} \rangle + \langle u_{v,\pm\mathbf{K}} | \hat{L}_\mp | u_{z,\pm\mathbf{K}} \rangle \langle u_{z,\pm\mathbf{K}} | z | u_{c,\pm\mathbf{K}} \rangle, \quad (\text{A9})$$

where only the coordinate parts of the wave functions enter (the spin part of the expression has been evaluated explicitly).

If we now substitute $u_{-\mathbf{K}}$ for all bands from equations (A1)–(A3) with $\varphi_c = \varphi_v$ following from (A7) and use $\hat{L}_-^* = -\hat{L}_+$ in the coordinate representation, we obtain $d_{-\mathbf{K}} = -d_{\mathbf{K}}^*$. At the same time, using equations (A4)–(A6) and noting that z remains invariant upon reflection $x \rightarrow -x$ while $\hat{L}_+ \rightarrow \hat{L}_-$, we obtain $d_{-\mathbf{K}} = d_{\mathbf{K}}$. As a result, $d_{-\mathbf{K}} = d_{\mathbf{K}} = id_z$ is purely imaginary, as in [48].

Appendix B: Block-diagonal form of the Rashba coupling

The 4×4 matrix $\mathcal{H}_\tau(\mathbf{k}) - \mathcal{E}_z \mathcal{D}_\tau$, can be transformed to the block-diagonal intra-band form by applying a unitary

transformation $e^{-\mathcal{S}_\tau(\mathbf{k})}$ (here \mathcal{E}_z is only the static electric field, while the same term with the optical field remains inter-band):

$$\tilde{\mathcal{H}}_\tau(\mathbf{k}) + \mathcal{H}^R(\mathbf{k}) = e^{-\mathcal{S}_\tau(\mathbf{k})} [\mathcal{H}_\tau(\mathbf{k}) - \mathcal{E}_z \mathcal{D}_\tau] e^{\mathcal{S}_\tau(\mathbf{k})} \quad (\text{B1})$$

If the matrix $\mathcal{S}_\tau(\mathbf{k})$ is chosen in the form

$$\mathcal{S}_{+1}(\mathbf{k}) = \frac{1}{E_g} \begin{bmatrix} 0 & 0 & -vk_- & 0 \\ 0 & 0 & -i\mathcal{E}_z d_z & -vk_- \\ vk_+ & -i\mathcal{E}_z d_z & 0 & 0 \\ 0 & vk_+ & 0 & 0 \end{bmatrix}, \quad (\text{B2})$$

$$\mathcal{S}_{-1}(\mathbf{k}) = \frac{1}{E_g} \begin{bmatrix} 0 & 0 & vk_+ & -i\mathcal{E}_z d_z \\ 0 & 0 & 0 & vk_+ \\ -vk_- & 0 & 0 & 0 \\ -i\mathcal{E}_z d_z & -vk_- & 0 & 0 \end{bmatrix}, \quad (\text{B3})$$

where $k_\pm = k_x \pm ik_y$, then, to the second order in $\mathcal{E}_z |d_z|/E_g \ll 1$, $vk/E_g \ll 1$, we obtain a block-diagonal Hamiltonian. The first term represents the kinetic energy of the electrons and holes,

$$\tilde{\mathcal{H}}_\tau(\mathbf{k}) = \begin{bmatrix} E_g + \tau\Delta_c\sigma_z + \frac{k^2}{2m_e} & 0 \\ 0 & \tau\Delta_v\sigma_z - \frac{k^2}{2m_h} \end{bmatrix}, \quad (\text{B4})$$

while the second one corresponds to the Rashba coupling,

$$\mathcal{H}^R(\mathbf{k}) = \frac{v\mathcal{E}_z}{E_g} d_z \begin{bmatrix} 0 & -ik_- & 0 & 0 \\ ik_+ & 0 & 0 & 0 \\ 0 & 0 & 0 & ik_- \\ 0 & 0 & -ik_+ & 0 \end{bmatrix}. \quad (\text{B5})$$

Here we also assumed $|\Delta_{c,v}| \ll E_g$. TMDC materials can have comparable values of the spin splitting in the valence band Δ_v and the gap E_g ; then the above calculation can be repeated without assuming $|\Delta_{c,v}| \ll E_g$, which would produce different Rashba coupling in the conduction and the valence band. For tungsten compounds $\Delta_v/E_g \sim 0.1$, so we neglect this difference. We also neglect the effect of the unitary transformation $e^{-\mathcal{S}_\tau(\mathbf{q})}$ on the Coulomb interaction which forms the excitonic states.

Appendix C: Estimate of the effective substrate-induced electric field

An external electric field \mathcal{E}_z and interaction with a substrate via van der Waals forces have the same qualitative effect of breaking the reflection symmetry in the z direction and deforming the electronic wave functions in the TMDC monolayer. Still, there is no reason for the deformation to be quantitatively similar in the two cases. Thus, characterization of the substrate effect by a single parameter, an effective \mathcal{E}_z , is quite a rough approximation, which gives only an order-of-magnitude estimate of the effect. Furthermore, we adopt a macroscopic description of the substrate, characterizing it by the dielectric constant. As the substrate is only a few angstroms away

from the monolayer center, such macroscopic description is also valid only qualitatively.

We model the TMDC monolayer as a slab of thickness d and dielectric constant ε , sandwiched between two media with dielectric constants ε_1 at $z > d/2$ and ε_2 at $z < -d/2$. Let us write the energy as a functional of the microscopic three-dimensional electronic density $\rho(\mathbf{R})$, $\mathbf{R} \equiv (\mathbf{r}, z)$ where the substrate effect is included as a Hartree-like term:

$$\begin{aligned} E[\rho(\mathbf{R})] = & E_0[\rho(\mathbf{R})] - \\ & - \int [V(\mathbf{R}, \mathbf{R}') - V_1(\mathbf{R}, \mathbf{R}')] \times \\ & \quad \times \rho(\mathbf{R}) \rho_i(\mathbf{R}') d^3\mathbf{R} d^3\mathbf{R}' + \\ & + \frac{1}{2} \int [V(\mathbf{R}, \mathbf{R}') - V_1(\mathbf{R}, \mathbf{R}')] \times \\ & \quad \times \rho(\mathbf{R}) \rho(\mathbf{R}') d^3\mathbf{R} d^3\mathbf{R}'. \end{aligned} \quad (\text{C1})$$

Here $E_0[\rho(\mathbf{R})]$ is the functional for a TMDC monolayer suspended in vacuum, $\rho_i(\mathbf{R}')$ is the ionic density (a sum of δ functions at the ion positions), $V(\mathbf{R}, \mathbf{R}')$ is the interaction potential, represented by the Green's function of the Poisson equation in the full dielectric structure multiplied by e^2 , $V_1(\mathbf{R}, \mathbf{R}')$ is the same for $\varepsilon_1 = \varepsilon_2 = 1$. The second and the third terms in Eq. (C1) describe interaction of the TMDC electrons with the polarization charges in the surrounding media. The deformed electronic wave functions can be found by varying the functional (C1). The whole description is analogous to the macroscopic description of polarons in ionic crystals [76]; indeed, deformation of electronic wave functions in the TMDC by interaction with a dielectric substrate can be viewed as a polaronic effect.

In the planar geometry considered here, evaluation of the integrals in Eq. (C1) reduces to a summation over image charges. When all three dielectric constants $\varepsilon, \varepsilon_1, \varepsilon_2$ are different, each charge produces an infinite number of images:

$$V(\mathbf{R}, \mathbf{R}') = \sum_{n=-\infty}^{\infty} \frac{\zeta_n e^2 / \varepsilon}{l_n}, \quad (\text{C2})$$

$$l_n = \sqrt{|\mathbf{r} - \mathbf{r}'|^2 + [z - (-1)^n z' - nd]^2}, \quad (\text{C3})$$

$$\zeta_0 = 1, \quad \zeta_{\pm 1} = \frac{\varepsilon - \varepsilon_{1,2}}{\varepsilon + \varepsilon_{1,2}}, \quad \zeta_{\pm 2} = \zeta_{\pm 1} \frac{\varepsilon - \varepsilon_{2,1}}{\varepsilon + \varepsilon_{2,1}}, \dots \quad (\text{C4})$$

For $\varepsilon_1 = \varepsilon_2 = 1 \ll \varepsilon$, the decay of ζ_n with $|n|$ is quite slow (which is a manifestation of the confinement of the electric field lines to the interior of the dielectric), so many images contribute to the Hartree terms in Eq. (C1). However, if we start with $\rho(\mathbf{R})$, symmetric with respect to $z \rightarrow -z$, the image charge distribution due to V_1 is also symmetric and does not produce any net electric field in the z direction. As concerns the V term, if at least one of $\varepsilon_1, \varepsilon_2$ is not small compared to ε , which we assume to be the case, ζ_n decays exponentially with a decrement ~ 1 . Thus, for an order-of-magnitude estimate, we can restrict ourselves to $\zeta_{\pm 1}$.

The electronic states we are interested in (the bottom of the conduction band and the top of the valence band at $\pm \mathbf{K}$ points) are known to originate mainly from d orbitals of the metal atoms. Assuming these orbitals to be concentrated around $z = 0$, we can expand the potentials in z/d as a formal small parameter. Of course, in reality the orbital spatial extent is of the same order as d , so this multipole expansion is good only for an order-of-magnitude estimate. The overall charge neutrality and the vanishing dipole moment of the unperturbed charge distribution around each metal atom (due to its D_{3h} symmetry) make the first non-vanishing multipolar moment to be the quadrupole. The quadrupole field decays with distance as $1/R^4$, so, even though each atom feels the field from images of all other atoms, the dominant contribution comes from the nearest two images which are due to the atom itself. The electric field at the point $\mathbf{R} = 0$ produced by the two quadrupole images at $\mathbf{R}' = (0, 0, \pm d)$ is given by

$$\mathcal{E}_z(0) = -\frac{3}{2} \frac{\zeta_1 - \zeta_{-1}}{\varepsilon d^4} Q_{zz}, \quad (\text{C5})$$

where Q_{zz} is the quadrupole moment of the electronic cloud around a single metal atom,

$$Q_{zz} \equiv -|e| \int (3z^2 - R^2) \rho(\mathbf{R}) d^3\mathbf{R}. \quad (\text{C6})$$

Although the quadrupole moment of a metal atom deformed by the crystal field differs from that of an isolated atom, we assume them to be of the same order and estimate the latter. The electronic configuration of tungsten is $[\text{Xe}]4f^{14}5d^46s^2$, and four out of five outermost d orbital states are filled, according to the Hund's rule. Since filled atomic shells have zero quadrupole moment, Q_{zz} for tungsten is determined by the single empty $5d$ orbital which we take to be the $m = 0$ one, as it is this one that is known to give rise to the lowest conduction band of tungsten dichalcogenides. The wave function of this orbital can be approximated by a hydrogen-like one with $(n, l, m) = (5, 2, 0)$, which moves in the Coulomb potential with effective charge $Z_{eff} = 16.74$ [77]. The average quadrupole moment of a hydrogenic $|n, l, m\rangle$ state [78],

$$\begin{aligned} Q_{zz} = & -|e| \frac{a_B^2}{Z_{eff}^2} \frac{n^2[5n^2 + 1 - 3l(l+1)]}{2} \times \\ & \times \frac{2l(l+1) - 6m^2}{4l(l+1) - 3}, \end{aligned} \quad (\text{C7})$$

then gives $Q_{zz} \approx 2.75 |e| a_B^2$ for tungsten ($a_B \approx 0.53 \text{ \AA}$ is the Bohr radius). For molybdenum, the electronic configuration in the gaseous phase, $[\text{Kr}]4d^55s^1$, has a filled $4d$ shell with zero quadrupole moment. However, given the fact that the lowest conduction band of molybdenum dichalcogenides is formed mostly by the $4d$ $m = 0$ orbital, just like for tungsten dichalcogenides, the electronic configuration is likely to be changed by the crystal field to $[\text{Kr}]4d^45s^2$. Then, repeating the same calculation with $(n, l, m) = (4, 2, 0)$, $Z_{eff} = 12.44$ [77], we obtain $Q_{zz} \approx 1.86 |e| a_B^2$ for molybdenum.

If a TMDC monolayer suspended in vacuum is subject to an *external* electric field \mathcal{E}_z , the field inside the monolayer is $\mathcal{E}_z/\varepsilon$. It is this one that should be matched with $\mathcal{E}_z(0)$ from Eq. (C5) to obtain the effective external field due to the substrate:

$$\mathcal{E}_z^{\text{eff}} = -\frac{3\varepsilon(\varepsilon_1 + \varepsilon_2)}{(\varepsilon + \varepsilon_1)(\varepsilon + \varepsilon_2)} \frac{Q_{zz}}{d^4}. \quad (\text{C8})$$

Taking the static dielectric constants $\varepsilon = 7$ (see [8] and references therein), $\varepsilon_1 = 1$ (vacuum), $\varepsilon_2 = 4$ (silica), and $d = 3.14 \text{ \AA}$, we obtain $\mathcal{E}_z^{\text{eff}} \sim -0.1 \text{ V/\AA}$ for tungsten dichalcogenides. Taking a highly dielectric substrate, $\varepsilon_2 \gg \varepsilon$, one can increase the effective field by about a factor of 2.

Appendix D: Electric field from the Maxwell equations and local field effects

Here we solve the Maxwell equations in the presence of the oscillating monolayer polarization $\mathbf{P}e^{i\mathbf{q}\mathbf{r}-i\omega t}\delta(z)$ sandwiched between two semi-infinite media with dielectric functions ε_1 and ε_2 occupying the half-spaces with $z > 0$ and $z < 0$, respectively. Due to the in-plane isotropy of the Maxwell equations and of the susceptibility, $\chi_{\alpha\beta} \propto \delta_{\alpha\beta}$, $\chi_{\alpha z} \propto q_\alpha$, we can assume the wave vector \mathbf{q} to be along the x axis, without any loss of generality. For the three-dimensional waves propagating in the two media, the z component of the wave vector is given by $q_{1z,2z} = \sqrt{\varepsilon_{1,2}\omega^2/c^2 - q^2}$.

For the s polarization, the fields in the incident, reflected and transmitted waves are parametrized by their electric field amplitudes \mathcal{E}_i , \mathcal{E}_r and \mathcal{E}_t , respectively. The non-zero components of the fields are given by (we omit the common factor $e^{iqx-i\omega t}$)

$$\mathcal{E}_y = \begin{cases} \mathcal{E}_i e^{-iq_{1z}z} + \mathcal{E}_r e^{iq_{1z}z}, & z > 0, \\ \mathcal{E}_t e^{-iq_{2z}z}, & z < 0, \end{cases} \quad (\text{D1})$$

$$B_x = \begin{cases} \frac{cq_{1z}}{\omega} (\mathcal{E}_i e^{-iq_{1z}z} - \mathcal{E}_r e^{iq_{1z}z}), & z > 0, \\ \frac{cq_{2z}}{\omega} \mathcal{E}_t e^{-iq_{2z}z}, & z < 0, \end{cases} \quad (\text{D2})$$

$$B_z = \frac{cq}{\omega} \mathcal{E}_y. \quad (\text{D3})$$

The boundary conditions on the tangential components of the electric and magnetic fields correspond to the continuity of the electric field and a jump in the magnetic field due to the surface current:

$$\mathcal{E}_i + \mathcal{E}_r - \mathcal{E}_t = 0, \quad (\text{D4})$$

$$\frac{cq_{1z}}{\omega} (\mathcal{E}_i - \mathcal{E}_r) - \frac{cq_{2z}}{\omega} \mathcal{E}_t = -\frac{4\pi i\omega}{c} P_y, \quad (\text{D5})$$

When the incident wave is absent, but the layer polarization acts as a source producing the outgoing field, the amplitudes of the latter are given by

$$\mathcal{E}_r = \mathcal{E}_t = \frac{4\pi i\omega^2}{c^2(q_{1z} + q_{2z})} P_y. \quad (\text{D6})$$

For the p polarization, we choose the magnetic field amplitudes B_i , B_r , B_t , to parametrize the fields, which are sought in the form

$$B_y = \begin{cases} B_i e^{-iq_{1z}z} + B_r e^{iq_{1z}z}, & z > 0, \\ B_t e^{-iq_{2z}z}, & z < 0, \end{cases} \quad (\text{D7})$$

$$\mathcal{E}_x = \begin{cases} \frac{cq_{1z}}{\varepsilon_1 \omega} (-B_i e^{-iq_{1z}z} + B_r e^{iq_{1z}z}), & z > 0, \\ -\frac{cq_{2z}}{\varepsilon_2 \omega} B_t e^{-iq_{2z}z}, & z < 0, \end{cases} \quad (\text{D8})$$

$$\mathcal{E}_z = \begin{cases} -\frac{cq}{\varepsilon_1 \omega} (B_i e^{-iq_{1z}z} + B_r e^{iq_{1z}z}), & z > 0, \\ -\frac{cq}{\varepsilon_2 \omega} B_t e^{-iq_{2z}z}, & z < 0. \end{cases} \quad (\text{D9})$$

The boundary conditions in this case are more subtle, because the z -polarization $P_z\delta(z)$ produces an electrical double layer. Let us assume $\delta(z)$ to be spread over a narrow but finite region $|z| < d/2$ (d being the monolayer thickness) with a background dielectric constant ε . In the first Maxwell equation for $\text{div}\mathbf{D}$,

$$iq\mathcal{E}_x + \frac{\partial\mathcal{E}_z}{\partial z} = -\frac{4\pi}{\varepsilon} iqP_x\delta(z) - \frac{4\pi}{\varepsilon} \frac{\partial}{\partial z} [P_z\delta(z)], \quad (\text{D10})$$

the first term is finite at $d \rightarrow 0$. In the layer region it can be neglected, which gives the following result for the field in the layer region (we omit the terms which vanish at $d \rightarrow 0$):

$$\mathcal{E}_x(z) = -\frac{cq}{\varepsilon\omega} B_t - \frac{4\pi}{\varepsilon} iqP_x \int_{-d/2}^z \delta(z') dz' - \frac{4\pi}{\varepsilon} P_z\delta(z), \quad (\text{D11})$$

where the first term represents the field at $z = -d/2+0^+$, related to the value at $z = -d/2-0^+$ from Eq. (D9) by the continuity of the normal component of the electric displacement.

In the third Maxwell equation for $\text{rot}\mathbf{B}$, the $\delta(z)$ term appears both in the polarization and displacement currents, so it cancels out, and the only singularity in $B_y(z)$ comes from the in-plane current,

$$B_y(z) = B_t + \frac{4\pi i\omega}{c} P_x \int_{-d/2}^z \delta(z') dz'. \quad (\text{D12})$$

However, from the Faraday's law,

$$\frac{\partial\mathcal{E}_x}{\partial z} - iq\mathcal{E}_z = \frac{i\omega}{c} B_y, \quad (\text{D13})$$

it follows that \mathcal{E}_x must have a jump of $-4\pi iqP_z/\varepsilon$:

$$\mathcal{E}_x(z) = -\frac{cq_{2z}}{\varepsilon_2\omega} B_t - \frac{4\pi}{\varepsilon} iqP_z \int_{-d/2}^z \delta(z') dz'. \quad (\text{D14})$$

This leads to the following boundary conditions for the amplitudes in Eqs. (D7)–(D9):

$$\frac{cq_{1z}}{\varepsilon_1\omega} (-B_i + B_r) + \frac{cq_{2z}}{\varepsilon_2\omega} B_t = -\frac{4\pi iq}{\varepsilon} P_z, \quad (\text{D15})$$

$$B_i + B_r - B_t = \frac{4\pi i\omega}{c} P_x. \quad (\text{D16})$$

If we wish to determine the outgoing field produced by a source layer polarization without the incident field, we have no ambiguity; the amplitudes are given by

$$B_x = \frac{4\pi i\omega}{c} \frac{(q_{2z}/\varepsilon_2)P_x - (q/\varepsilon)P_z}{q_{1z}/\varepsilon_1 + q_{2z}/\varepsilon_2}, \quad (\text{D17})$$

$$B_z = \frac{4\pi i\omega}{c} \frac{-(q_{1z}/\varepsilon_1)P_x - (q/\varepsilon)P_z}{q_{1z}/\varepsilon_1 + q_{2z}/\varepsilon_2}. \quad (\text{D18})$$

However, we face a problem when we want to couple the field back to the polarization, as we need the value $\mathcal{E}_{x,z}(z=0)$, which is undetermined due to the singularity. Here we note that coupling to the layer polarization is in fact determined by $\int \delta(z) \mathcal{E}_{x,z}(z) dz$, with the same $\delta(z)$ as in the spatial profile of the polarization itself, which is nothing but the product of the microscopic wave functions of the electron and the hole at coinciding points (see, e. g., a microscopic treatment for excitons in a semiconductor quantum well [38, 49]). In other words, we define

$$\bar{D}_{ij}(\mathbf{q}, \omega) = \int \delta(z) D_{ij}(z, z'; \mathbf{q}, \omega) \delta(z') dz dz', \quad (\text{D19})$$

i. e., as the projection on the polarization spatial profile in the z direction. Then, the uncertainty due to the integral terms in Eqs. (D11), (D14) is resolved as

$$\int_{-d/2}^{d/2} dz \int_{-d/2}^z dz' \delta(z) \delta(z') = \frac{1}{2}, \quad (\text{D20})$$

by symmetry. On the contrary, the term

$$\int_{-d/2}^{d/2} \delta^2(z) dz \equiv \frac{\kappa_0}{2\varepsilon} \sim \frac{1}{d} \quad (\text{D21})$$

can only be determined from the microscopic theory. The projected fields are given by

$$\int \delta(z) \mathcal{E}_x(z) dz = \frac{2(q_{1z}/\varepsilon_1)(q_{2z}/\varepsilon_2)}{q_{1z}/\varepsilon_1 + q_{2z}/\varepsilon_2} 2\pi i P_x + \frac{q}{\varepsilon} \frac{q_{2z}/\varepsilon_2 - q_{1z}/\varepsilon_1}{q_{1z}/\varepsilon_1 + q_{2z}/\varepsilon_2} 2\pi i P_z, \quad (\text{D22})$$

$$\int \delta(z) \mathcal{E}_z(z) dz = \frac{q}{\varepsilon} \frac{q_{1z}/\varepsilon_1 - q_{2z}/\varepsilon_2}{q_{1z}/\varepsilon_1 + q_{2z}/\varepsilon_2} 2\pi i P_x - \frac{2\pi\kappa_0}{\varepsilon^2} P_z + \frac{2(q/\varepsilon)^2}{q_{1z}/\varepsilon_1 + q_{2z}/\varepsilon_2} 2\pi i P_z. \quad (\text{D23})$$

To arrive at the final expressions (33)–(35), one should recall that the field \mathcal{E}_z which appears in the definition of the dipole moment (8), and which was used in the Rashba coupling constant estimate of [46], is not the local field, but the external field, applied to a monolayer suspended in vacuum. Hence, a factor $1/\varepsilon$ should be absorbed into d_z .

Appendix E: Radiative rates in a parallel magnetic field

As the s and p polarizations do not separate in a parallel magnetic field, we return to the valley basis. Namely, instead of using Eq. (37), we represent the susceptibility near each pole E_ν as

$$\chi_{ij}(\mathbf{q}, \omega) \approx \sum_{\tau=\pm 1} \frac{\mu_{\tau i}^\nu (\mu_{\tau j}^\nu)^*}{E_\nu - \omega + i0^+}, \quad (\text{E1})$$

where the vector μ_τ^ν , describes the polarization of the exciton ν in the valley τ . Then, the radiative self-energy can be approximated by

$$\Sigma_{\tau\tau'}^\nu(\mathbf{q}) = -(\mu_{\tau i}^\nu)^* \bar{D}_{ij}(\mathbf{q}, E_\nu) \mu_{\tau' j}^\nu. \quad (\text{E2})$$

For the dark A excitons in the parallel magnetic field, these vectors are given by

$$\mu_{+1} = -i \frac{ev\Phi(0)}{E_A^d} \frac{g_{\parallel} \mu_B B_-}{4\Delta_c} (\mathbf{e}_x + i\mathbf{e}_y) + id_z \Phi(0) \mathbf{e}_z, \quad (\text{E3})$$

$$\mu_{-1} = i \frac{ev\Phi(0)}{E_A^d} \frac{g_{\parallel} \mu_B B_+}{4\Delta_c} (\mathbf{e}_x - i\mathbf{e}_y) + id_z \Phi(0) \mathbf{e}_z, \quad (\text{E4})$$

where $B_\pm = B_x \pm iB_y$. As we have seen in Sec. IV B, the most important term that lifts the valley splitting is the last term in Eq. (35). Thus, we first consider the splitting at $\mathbf{q} = 0$, $\mathbf{B}_{\parallel} = 0$, determined by the self-energy matrix

$$\Sigma^{(0)}(\mathbf{q} = 0) = \frac{\Xi_0}{2} \begin{bmatrix} 1 & 1 \\ 1 & 1 \end{bmatrix}, \quad (\text{E5})$$

Its eigenvectors determine the z -dipole-active state $(1, 1)^T/\sqrt{2}$ whose energy is shifted up by Ξ_0 , and the orthogonal one, $(1, -1)^T/\sqrt{2}$, which is z -dipole-inactive. In the case of Rashba-induced splitting at $\mathbf{q} \neq 0$ these states evolve into the p - and s -polarized ones, respectively. At finite \mathbf{q} and \mathbf{B}_{\parallel} , we project the self-energy on the two eigenvectors $(1, \pm 1)^T/\sqrt{2}$, which gives the radiative shift and the decay rate of the two states

$$\begin{aligned} \Omega_{\perp}(\mathbf{q}) - \frac{i}{2} \Gamma_{\perp}(\mathbf{q}) &= -8\pi i \Phi^2(0) \frac{e^2 v^2}{E_A^2} \left(\frac{g_{\parallel} \mu_B B_{\parallel}}{4\Delta_c} \right)^2 \times \\ &\times \left[\frac{(E_A/c)^2}{q_{1z}^A + q_{2z}^A} \cos^2 \tilde{\phi} + \frac{(q_{1z}^A/\varepsilon_1)(q_{2z}^A/\varepsilon_2)}{q_{1z}^A/\varepsilon_1 + q_{2z}^A/\varepsilon_2} \sin^2 \tilde{\phi} \right] - \\ &- 4\pi \Phi^2(0) \frac{evd_z}{E_A} \frac{g_{\parallel} \mu_B B_{\parallel}}{4\Delta_c} \frac{q_{1z}^A/\varepsilon_1 - q_{2z}^A/\varepsilon_2}{q_{1z}^A/\varepsilon_1 + q_{2z}^A/\varepsilon_2} q \sin \tilde{\phi} - \\ &- \frac{8\pi i q^2 d_z^2 \Phi^2(0)}{q_{1z}^A/\varepsilon_1 + q_{2z}^A/\varepsilon_2} + \Xi_0, \end{aligned} \quad (\text{E6})$$

$$\begin{aligned} \Omega_{\parallel}(\mathbf{q}) - \frac{i}{2} \Gamma_{\parallel}(\mathbf{q}) &= -8\pi i \Phi^2(0) \frac{e^2 v^2}{E_A^2} \left(\frac{g_{\parallel} \mu_B B_{\parallel}}{4\Delta_c} \right)^2 \times \\ &\times \left[\frac{(E_A/c)^2}{q_{1z}^A + q_{2z}^A} \sin^2 \tilde{\phi} + \frac{(q_{1z}^A/\varepsilon_1)(q_{2z}^A/\varepsilon_2)}{q_{1z}^A/\varepsilon_1 + q_{2z}^A/\varepsilon_2} \cos^2 \tilde{\phi} \right], \end{aligned} \quad (\text{E7})$$

where $\tilde{\phi} = \phi_{\mathbf{q}} - \phi_{\mathbf{B}}$, and $\phi_{\mathbf{q}}, \phi_{\mathbf{B}}$ are the polar angles of \mathbf{q} and \mathbf{B}_{\parallel} in the xy plane, respectively.

Appendix F: Momentum integration of the decay rates

It is convenient to introduce a dimensionless variable $s = c^2 q^2 / E_A^2$, then the integration over \mathbf{q} transforms as $\int d^2 \mathbf{q} = \pi (E_A / c)^2 \int ds$, and the radiative decay rates of the A excitons, given by Eqs. (39), (40), (41), (E6), (E7), can be written as

$$\frac{\Gamma_{TA}^b}{\Gamma_0} = \text{Re} \frac{2}{\sqrt{\varepsilon_1 - s} + \sqrt{\varepsilon_2 - s}}, \quad (\text{F1})$$

$$\frac{\Gamma_{TA}^d}{\Gamma_0} = \eta_R \text{Re} \frac{2s}{\sqrt{\varepsilon_1 - s} + \sqrt{\varepsilon_2 - s}}, \quad (\text{F2})$$

$$\frac{\Gamma_{LA}^b}{\Gamma_0} = \text{Re} \frac{2\sqrt{\varepsilon_1 - s}\sqrt{\varepsilon_2 - s}}{\varepsilon_2\sqrt{\varepsilon_1 - s} + \varepsilon_1\sqrt{\varepsilon_2 - s}}, \quad (\text{F3})$$

$$\frac{\Gamma_{LA}^d}{\Gamma_0} = \eta_z \text{Re} \frac{2\varepsilon_1\varepsilon_2 s}{\varepsilon_2\sqrt{\varepsilon_1 - s} + \varepsilon_1\sqrt{\varepsilon_2 - s}}, \quad (\text{F4})$$

where we keep only the dominant terms. It is convenient to get rid of the square roots in the denominators and take the real part of each term in the numerators separately. Then the integration becomes straightforward and gives

$$\int \frac{d^2 \mathbf{q}}{(2\pi)^2} \frac{\Gamma_{TA}^b(\mathbf{q})}{\Gamma_0} = \frac{(E_A/c)^2}{2\pi} \frac{2}{3} \frac{\varepsilon_2^{3/2} - \varepsilon_1^{3/2}}{\varepsilon_2 - \varepsilon_1}, \quad (\text{F5})$$

$$\int \frac{d^2 \mathbf{q}}{(2\pi)^2} \frac{\Gamma_{TA}^d(\mathbf{q})}{\Gamma_0} = \eta_R \frac{(E_A/c)^2}{2\pi} \frac{4}{15} \frac{\varepsilon_2^{5/2} - \varepsilon_1^{5/2}}{\varepsilon_2 - \varepsilon_1}, \quad (\text{F6})$$

$$\begin{aligned} \int \frac{d^2 \mathbf{q}}{(2\pi)^2} \frac{\Gamma_{LA}^b(\mathbf{q})}{\Gamma_0} &= \frac{(E_A/c)^2}{2\pi} \left[\frac{2}{3} \frac{\varepsilon_2^{5/2} - \varepsilon_1^{5/2}}{\varepsilon_2^2 - \varepsilon_1^2} - \right. \\ &\quad \left. - \frac{2(\varepsilon_1\varepsilon_2)^{3/2}(\sqrt{\varepsilon_2} - \sqrt{\varepsilon_1})}{(\varepsilon_2^2 - \varepsilon_1^2)(\varepsilon_2 + \varepsilon_1)} - \frac{2\varepsilon_1^2\varepsilon_2^2}{(\varepsilon_2^2 - \varepsilon_1^2)(\varepsilon_1 + \varepsilon_2)^{3/2}} \times \right. \\ &\quad \left. \times \ln \left(\sqrt{\frac{\varepsilon_2}{\varepsilon_1}} \frac{\sqrt{\varepsilon_2 + \varepsilon_1} + \sqrt{\varepsilon_2}}{\sqrt{\varepsilon_2 + \varepsilon_1} + \sqrt{\varepsilon_1}} \right) \right], \quad (\text{F7}) \end{aligned}$$

$$\begin{aligned} \int \frac{d^2 \mathbf{q}}{(2\pi)^2} \frac{\Gamma_{LA}^d(\mathbf{q})}{\Gamma_0} &= \eta_z \frac{(E_A/c)^2}{2\pi} \left[\frac{2\varepsilon_1^2\varepsilon_2^2}{(\varepsilon_1 + \varepsilon_2)^2} \times \right. \\ &\quad \times \frac{\sqrt{\varepsilon_1\varepsilon_2} + (\varepsilon_1 + \varepsilon_2)/3}{\sqrt{\varepsilon_1} + \sqrt{\varepsilon_2}} + \frac{2\varepsilon_1^3\varepsilon_2^3}{(\varepsilon_2^2 - \varepsilon_1^2)(\varepsilon_1 + \varepsilon_2)^{3/2}} \times \\ &\quad \left. \times \ln \left(\sqrt{\frac{\varepsilon_2}{\varepsilon_1}} \frac{\sqrt{\varepsilon_2 + \varepsilon_1} + \sqrt{\varepsilon_2}}{\sqrt{\varepsilon_2 + \varepsilon_1} + \sqrt{\varepsilon_1}} \right) \right]. \quad (\text{F8}) \end{aligned}$$

The function $\mathcal{F}_T^d(\varepsilon_1, \varepsilon_2) \equiv (4/15)(\varepsilon_2^{5/2} - \varepsilon_1^{5/2})(\varepsilon_2 - \varepsilon_1)$, the function $\mathcal{F}_L^d(\varepsilon_1, \varepsilon_2)$ is given by the square bracket in Eq. (F8), and $\mathcal{F}^b(\varepsilon_1, \varepsilon_2)$ is given by the half-sum of $(2/3)(\varepsilon_2^{3/2} - \varepsilon_1^{3/2})(\varepsilon_2 - \varepsilon_1)$ and the square bracket in Eq. (F7).

[1] Splendiani A, Sun L, Zhang Y, Li T, Kim J, Chim C Y, Galli G and Wang F 2010 *Nano Lett.* **10** 1271
[2] Mak K F, Lee C, Hone J, Shan J and Heinz T F, 2010 *Phys. Rev. Lett.* **105** 136805
[3] Novoselov K S, Jiang D, Schedin F, Booth T J, Khotkevich V V, Morozov S V and Geim A K 2005 *PNAS* **102** 16188
[4] Zhan Y, Liu Z, Najmaei S, Ajayan P M and Lou J 2012 *Small* **8** 966

[5] Liu K K, Zhang W, Lee Y H, Lin Y C, Chang M T, Su C Y, Chang C S, Li H, Shi Y, Zhang H, Lai C S and Li L J 2012 *Nano. Lett.* **12** 1538
[6] Zhang Y, Chang T R, Zhou B, Cui Y T, Yan H, Liu Z, Schmitt F, Lee J, Moore R, Chen Y, Lin H, Jeng H T, Mo S K, Hussain Z, Bansil A and Shen Z X 2014 *Nature Nanotech.* **9** 111
[7] Ramasubramaniam A 2012 *Phys. Rev. B* **86** 115409

- [8] Berkelbach T C, Hybertsen M S and Reichman D R 2013 *Phys. Rev. B* **88** 045318
- [9] Qiu D Y, da Jornada F H and Louie S G 2013 *Phys. Rev. Lett.* **111** 216805
- [10] Chernikov A, Berkelbach T C, Hill H M, Rigosi A, Li Y, Aslan O B, Reichman D R, Hybertsen M S and Heinz T F 2014 *Phys. Rev. Lett.* **113** 076802
- [11] Ye Z, Cao T, O'Brien K, Zhu H, Yin X, Wang Y, Louie S G and Zhang X 2014 *Nature* **513** 214
- [12] He K, Kumar N, Zhao L, Wang Z, Mak K F, Zhao H and Shan J 2014 *Phys. Rev. Lett.* **113** 026803
- [13] Zhu B, Chen X and Cui X 2015 *Scientific Reports* **5** 9218
- [14] Eda G and Maier S A 2014 *ACS Nano* **7** 5660
- [15] Xiao D, Liu G B, Feng W, Xu X and Yao W 2012 *Phys. Rev. Lett.* **108** 196802
- [16] Yao W, Xiao D and Niu Q 2008 *Phys. Rev. B* **77** 235406
- [17] Cao T, Wang G, Han W, Ye H, Zhu C, Shi J, Niu Q, Tan P, Wang E, Liu B and Feng J 2012 *Nature Commun.*, **3** 887
- [18] Zeng H, Dai J, Yao W, Xiao D and Cui X 2012 *Nature Nanotech.* **7** 490
- [19] Mak K F, He K, Shan J and Heinz T F 2012 *Nature Nanotech.* **7** 494
- [20] Sallen G, Bouet L, Marie X, Wang G, Zhu C R, Han W P, Lu Y, Tan P H, Amand T, Liu B L and Urbaszek B 2012 *Phys. Rev. B* **86** 081301(R)
- [21] Jones A M, Yu H, Ghimire N J, Wu S, Aivazian G, Ross J S, Zhao B, Yan J, Mandrus D G, Xiao D, Yao W and Xu X 2013 *Nature Nano.* **8** 634
- [22] Wang G, Bouet L, Lagarde D, Vidal M, Balocchi A, Amand T, Marie X and Urbaszek B 2014 *Phys. Rev. B* **90** 075413
- [23] Rivera P, Seyler K L, Yu H, Schaibley J R, Yan J, Mandrus D G, Yao W and Xu X 2016 *Science* **351** 688
- [24] Hao K, Moody G, Wu F, Dass C K, Xu L, Chen C H, Sun L, Li M Y, Li L J, MacDonald A H and Li X 2016 *Nature Phys.*
- [25] Kormányos A, Zólyomi V, Drummond N D, Rakyta P, Burkard G and Fal'ko V I 2013 *Phys. Rev. B* **88** 045416
- [26] Liu G B, Shan W Y, Yao Y, Yao W and Xiao D 2013 *Phys. Rev. B* **88** 085433
- [27] Kořmider K, González J W and Fernández-Rossier J 2013 *Phys. Rev. B* **88** 245436
- [28] Arora A, Koperski M, Nogajewski K, Marcus J, Faugeras C and Potemski M 2010 *Nanoscale* **105** 136805
- [29] Withers F, Del Pozo-Zamudio O, Schwarz S, Dufferwiel S, Walker P M, Godde T, Rooney A P, Gholinia A, Woods C R, Blake P, Haigh S J, Watanabe K, Taniguchi T, Aleiner I L, Geim A K, Fal'ko V I, Tartakovskii A I and Novoselov K S 2015 *Nano Lett.* **15** 8223
- [30] Wang G, Robert C, Suslu A, Chen B, Yang S, Alamdari S, Gerber I C, Amand T, Marie X, Tongay S and Urbaszek B 2015 *Nature Comm.* **6** 10110
- [31] Zhang X X, You Y, Zhao S Y F and Heinz T F 2015 *Phys. Rev. Lett.* **115** 257403
- [32] You Y, Zhang X X, Berkelbach T C, Hybertsen M S, Reichman D R and Heinz T F 2015 *Nature Phys.* **11** 477
- [33] Mitioglu A A, Plochocka P, Granados del Aguila Á, Christianen P C M, Deligeorgis G, Anghel S, Kulyuk L and Maude D K 2015 *Nano Lett.* **15** 4387
- [34] Koperski M, Nogajewski K, Arora A, Cherkez V, Mallet P, Veuillen J Y, Marcus J, Kossacki P and Potemski M 2015 *Nature Nanotech.* **10** 503
- [35] Srivastava A, Sidler M, Allain A V, Lembke D S, Kis A and Imamoglu A 2015 *Nature Nanotech.* **10** 491
- [36] Smoleński T, Goryca M, Koperski M, Faugeras C, Kazimierzczuk T, Nogajewski K, Kossacki P and Potemski M 2015 *Phys. Rev. X* **6** 021024
- [37] Agranovich V M and Dubovskii O A 1966 *Pis'ma ZhETF* **3** 345 [1966 *JETP Lett.* **3** 223]
- [38] Andreani L C and Bassani F 1990 *Phys. Rev. B* **41** 7536
- [39] Andreani L C, Tassone F and Bassani F 1991 *Solid State Commun.* **77** 641
- [40] Glazov M M, Amand T, Marie X, Lagarde D, Bouet L and Urbaszek B 2014 *Phys. Rev. B* **89** 201302(R)
- [41] Gartstein Yu N, Li X and Zhang C 2015 *Phys. Rev. B* **92** 075445
- [42] Palummo M, Bernardi M and Grossman J C 2015 *Nano Lett.* **15** 2794
- [43] Wang H, Zhang C, Chan W, Manolatu C, Tiwari S and Rana F 2016 *Phys. Rev. B* **93** 045407
- [44] Bychkov Yu A and Rashba E I 1984 *J. Phys. C: Solid State Phys.* **17** 6039
- [45] Dery H and Song Y 2015 *Phys. Rev. B* **92** 125431
- [46] Kormányos A, Zólyomi V, Drummond N D and Burkard G 2014 *Phys. Rev. X* **4** 011034
- [47] Echeverry J P, Urbaszek B, Amand T, Marie X and Gerber I C 2016 *Phys. Rev. B* **93** 121107(R)
- [48] Ochoa H and Roldán R 2013 *Phys. Rev. B* **87** 245421
- [49] Chen Y, Gil B, Lefebvre P and Mathieu H 1988 *Phys. Rev. B* **37** 6429
- [50] Kormányos A, Burkard G, Gmitra M, Fabian J, Zólyomi V, Drummond N D and Fal'ko V 2015 *2D Mater.* **2** 022001
- [51] Mattheiss L F 1973 *Phys. Rev. B* **8** 3719
- [52] Voß D, Krüger P, Mazur A and Pollmann J 1999 *Phys. Rev. B* **60** 14311
- [53] Lebègue S and Eriksson O 2009 *Phys. Rev. B* **79** 115409
- [54] Zhu Z Y, Cheng Y C and Schwingenschlögl U 2011 *Phys. Rev. B* **84** 153402
- [55] Kadantsev E S and Hawrylak P 2012 *Solid State Commun.* **152** 909
- [56] Chang C H, Fan X, Lin S H and Kuo J L 2013 *Phys. Rev. B* **88** 195420
- [57] Cappelluti E, Roldán R, Silva-Guillén J A, Ordejón P and Guinea F 2013 *Phys. Rev. B* **88** 075409
- [58] Song Y and Dery H 2013 *Phys. Rev. Lett.* **111**, 026601
- [59] Stier A V, McCreary K M, Jonker B T, Kono J and Crooker S A 2016 *Nat. Comm.* **7** 10643
- [60] One might try to improve the precision of (20) by replacing $E_g \rightarrow E_g - E_b - \tau_{s_v} \Delta_v$ in the denominator which represents the interband excitation energy; indeed, the excion binding energy E_b is known to be quite large in TMDCs, values up to $E_b \sim 1$ eV having been reported [7–13]. However, if one corrects the denominator in (20), then, to be consistent, one would also have to correct that in (4), as well as to go beyond the parabolic approximation for the electron and hole dispersion. Thus, to be systematic, we assume to be in the limit $E_b \ll E_g$ and neglect corrections of the order of E_b/E_g and higher. Beyond this limit (the extreme case being that of Frenkel excitons), one can still work with the effective excitonic Hamiltonian (19), however, its parameters have no simple relation with the single-electron band structure parameters.
- [61] In fact, the energy difference between the dark and bright excitons does not necessarily coincide with the single-

particle spin splitting in the conduction band, due to an extra contribution from the exchange interaction [47]. Here, $2\Delta_c$ should be understood as the excitonic splitting.

- [62] Abrikosov A A, Gor'kov L P and Dzyaloshinskii I Ye 1965 *Quantum Field Theoretical Methods in Statistical Physics* (Pergamon Press, Oxford)
- [63] Note that for $\varepsilon_1 = \varepsilon_2$, the denominator in Eq. (39) can vanish; in this case, the perturbative approach (38) is not valid, so a more precise analysis of the original dispersion Eq. (32) is required [37]. Here we assume ε_1 and ε_2 to differ significantly, so this problem does not arise.
- [64] Note that because $\varepsilon_1 \neq \varepsilon_2$, for q between $\sqrt{\varepsilon_1}E_A/c$ and $\sqrt{\varepsilon_2}E_A/c$, one of the square roots in q_{1z}^A, q_{2z}^A is real, while the other is imaginary, so separation of the real and imaginary parts in (39), (40), (41) must be done with caution. We do not give explicit expressions for Ω and Γ separately, as they would be much more bulky than the combined expressions for $\Omega - (i/2)\Gamma$.
- [65] Yu H, Liu G-B, Gong P, Xu X and Yao W 2014 *Nature Comm.* **5** 3876
- [66] Yu H, Cui X, Xu X and Yao W 2015 *Natl. Sci. Rev.* **2** 57
- [67] In fact, lifting of the valley degeneracy for the dark A excitons follows from a very simple and general consideration. Consider the states at $\mathbf{q} = 0$ in the absence of external fields. Then, we have two degenerate excitations corresponding to the $\pm\mathbf{K}$ valleys, whose transition dipole moments are both directed along z . Then, it is always possible to form two linear combinations of them, one of which will have zero dipole moment and zero decay rate, while for the other one they will be finite. If the decay rates for the two states are different, so must be the energy shifts, which means lifting of the degeneracy.
- [68] Ferrini R, Patirini M and Franchi S 1998 *J. Appl. Phys.* **84** 4517
- [69] Piermarocchi C, Tassone F, Savona V, Quattropani A and Schwendimann P 1996 *Phys. Rev. B* **53** 15834
- [70] Slobodeniuk A O and Basko D M 2016 *Phys. Rev. B* **94** 205423
- [71] Moody G, Dass C K, Hao K, Chen C-H, Li L-J, Singh A, Tran K, Clark G, Xu X, Berghuser G, Malic E, Knorr A and Li X 2015 *Nat. Commun.* **6** 8315
- [72] Koirala S, Mouri S, Miyauchi Y and Matsuda K 2016 *Phys. Rev. B* **93** 075411
- [73] Dey P, Paul J, Wang Z, Stevens C E, Liu C, Romero A H, Shan J, Hilton D J and Karaiskaj D 2016 *Phys. Rev. Lett.* **116** 127402
- [74] Selig M, Berghäuser G, Raja A, Nagler P, Schüller C, Heinz T F, Korn T, Chernikov A, Malic E and Knorr A 2016 *arXiv:1605.03359*
- [75] Jakubczyk T, Delmonte V, Koperski M, Nogajewski K, Faugeras C, Langbein W, Potemski M and Kasprzak J 2016 *arXiv:1606.07634*
- [76] Pekar S 1946 *Zh. Eksp. Teor. Fiz.* **16** 341
- [77] Clementi E, Raimondi D L and Reinhardt W P 1967 *J. Chem. Phys.* **47** 1300
- [78] Bethe H A and Salpeter E M 1957 *Quantum mechanics of one- and two-electron atoms*, (Springer-Verlag, Berlin)